Interferon adjusts stem cell output in the young and old brain to meet demand independently of its antiviral function

Damian Carvajal Ibañez[1,2,12], Maxim Skabkin[1,12], Jooa Hooli[1,2,3,12], Santiago Cerrizuela[1], Manuel Göpferich[1,2,9], Adrien Jolly[4], Marc Zumwinkel[1,10], Matilde Bertolini[5,11], Thomas Höfer[4], Guenter Kramer[5], Simon Anders[6], Aurelio Telemann[7], Anna Marciniak-Czochra[3,8,*], Ana Martin-Villalba[1,13,*]

[1]Division of Molecular Neurobiology, German Cancer Research Center (DKFZ), Heidelberg 69120, Germany
[2]Faculty of Biosciences, Heidelberg University, Heidelberg 69120, Germany
[3]Institute of Applied Mathematics, Heidelberg University, Heidelberg 69120, Germany
[4]Division of Theoretical Systems Biology, German Cancer Research Center (DKFZ), Heidelberg 69120, Germany
[5]Center for Molecular Biology of Heidelberg University (ZMBH) & German Cancer Research Center (DKFZ), DKFZ-ZMBH Alliance, Heidelberg 69120, Germany
[6]Bioquant, Heidelberg University, Heidelberg 69120, Germany
[7]Division of Signal Transduction in Cancer and Metabolism, German Cancer Research Center (DKFZ), Heidelberg 69120, Germany
[8]Interdisciplinary Center of Scientific Computing (IWR) and Bioquant, Heidelberg University, Heidelberg 69120, Germany
[9]Currently at: CureVac N.V., Tübingen 72076, Germany
[10]Currently at: Institute for Medical Microbiology and Hygiene, University Hospital Ulm, Ulm 89081, Germany
[11]Currently at: Department of Genetics, Stanford University School of Medicine: Stanford, CA 94305, USA
[12]These authors contributed equally
[13]Lead contact
[*]Correspondence: a.martin-villalba@dkfz-heidelberg.de; anna.marciniak@iwr.uni-heidelberg.de

Summary

Stem cells show intrinsic interferon signaling, which protects them from viral infections. In the brain, type I interferon signaling increases in stem cells as they age and reduces their ability to become activated for repair. Whether interferons impact stem cell activity only in aging, how, and if it is coupled to the intrinsic immune function remains elusive. Our study shows that interferon-β arrested stem cells in G_0 of the cell cycle and transiently increased their TOR signaling before switching it off. This bimodal regulation of TOR is needed to repress translation of Sox2. Single-cell transcriptomics reveals that in the absence of interferon receptors, interferon signaling levels change and its increase with age disappears. Mathematical simulations indicate that interferons are beneficial in the young and harmful in the old brain. Our study identifies interferons as genuine regulators of stem cell homeostasis and potential therapeutic target to repair the aging brain.

Keywords

neural stem cells, interferon, stem cell aging, quiescence, adult neurogenesis, intrinsic interferon signature, antiviral mechanisms, modeling, simulations.

Introduction

Interferons (IFNs) are cytokines known to modulate the innate and adaptive immune response upon infections and injury (Mazewski, Perez, Fish, & Platanias, 2020). The interferon family is composed of type I, II and III IFNs. While type I and II IFNs are sensed ubiquitously in the body, type III IFN response is restricted to immune and epithelial cells. Type I and II IFNs activate the canonical JAK/STAT signaling pathway through IFN receptor α (IFNRA) and γ (IFNRG), respectively, leading to the transcription of a subset of interferon stimulated genes (ISGs)(Alspach, Lussier, & Schreiber, 2019; Stanifer, Guo, Doldan, & Boulant, 2020). Despite the ubiquitous expression of IFNAR and IFNGR in stem cells, they show an attenuated response to IFN compared to differentiated counterparts (Wu et al., 2018; Wu, Kwong, & Rice, 2019). Instead, stem cells, including neural stem cells (NSCs), rely on intrinsic expression of ISGs to prevent viral infection (Wu et al., 2018). Upon differentiation, this intrinsic ISG expression disappears and the ability to respond to IFN ligands is acquired (Wu et al., 2018). We and others have found increased expression of type I-related ISGs in NSCs and their neighboring cells in the old brain (Baruch et al., 2014; Kalamakis et al., 2019). This increased ISG expression is associated with a decreased rate of NSCs activation, which prevents their full depletion but at the same time compromises their repair capacity (Kalamakis et al., 2019). Understanding how the positive and negative functions of interferon are molecularly wired in stem cells is mandatory to provide a better aging.

Results

Interferon regulates stemness at all ages and halts NSCs in G_0

We first addressed whether the age-dependent change in stem cell activity is caused by intrinsic or interferon dependent signaling. In addition, we addressed the relevance of this regulation to stem cells in the young brain. To this end, we examined NSC dynamics in mice lacking the IFNA and IFNG receptors, referred to as IFNAGR KO. To this end, we quantified the pool of NSCs (Prom1$^+$GLAST$^+$) within the ventricular-subventricular zone (vSVZ) via flow cytometry and compared them to wild-type (WT) controls. In addition, we used the fraction of active NSCs, i.e., the number of cycling cells among the BrdU-retaining cells, previously acquired in WT and IFNAGR KO animals[3]. These data were analyzed using a mathematical model previously

established and validated in wild-type animals (Kalamakis et al., 2019). Such model describes the dynamics of quiescent, active and neurogenic progenitor populations and allows linking those to age-dependent changes in the cell parameters: (i) activation rate and (ii) self-renewal probability (Figure 1A, Supplementary Data). For wild-type data, as already reported (Kalamakis et al., 2019), it pointed to a profound reduction of the NSC activation rate and a slight increase in self-renewal probability as the parameters responsible for a deceleration in NSC decline in old mice. Notably, this deceleration is needed to maintain a minimal amount of NSCs that otherwise would be fully depleted at older ages. In IFNAGR KO, NSC depletion exhibited faster dynamics and yet stabilized at counts of around 150 cells per mouse, as in WT mice (Figure 1B). The mathematical model applied to the IFNAGR KO data predicted a constant activation rate of NSCs and an earlier time-dependent regulation of the probability of NSC self-renewal (Figure 1C). The latter explained the observed saturation in the NSC decline. This unveils self-renewal as a second layer of regulation, following modulation of the activation rate.

Next, we wanted to address how IFN regulates quiescence at the molecular level. As the highest degree of quiescence is shown in the aging brain, and here the predominant activity is type I IFN (IFN-α & -β) response (Baruch et al., 2014), we assessed exposure to IFN-β. We previously showed that NSCs exposed to IFN type I stop cycling (Kalamakis et al., 2019). We now addressed how IFN impacts cell cycle with Cycleflow[10], which infers the length of the cell cycle stages and the distribution of cells in each stage including quiescence (G_0). The Cycleflow model assumes that cell cycle is not changing during the experiment. Hence, we pre-treated NSCs with IFN-β for 18 hours, after which NSCs stably reduce their cycling activity (Figure S1). We then followed the cells for up to 36 hours in the presence or absence of IFN-β (Figure 1D). We found that the overall estimated population growth was profoundly decreased, which correlated with an increase in G_1 length and accumulation of NSCs in G_0. Thus, long exposure to IFN-β shifts NSCs to a quiescent G_0 state, which is consistent with the predictions of our mathematical model linking the IFN function with NSC activation.

IFN-β exerts a biphasic control of mRNA translation

In addition to restricting proliferation, interferons modulate mRNA translation (Mazewski et al., 2020). This process is of key importance in the regulation of

quiescence in stem cells (Baser et al., 2019; Baser, Skabkin, & Martin-Villalba, 2017; Blanco et al., 2016; Tahmasebi, Amiri, & Sonenberg, 2019). We thus hypothesized that IFN-β could also affect mRNA translation in NSCs. To address this, we examined polysome profiles and ribosome footprinting (Ribo-Seq) of NSCs following short (2h) or long (14h) exposure to IFN-β. Analysis of the polysome profiles of IFN-β-treated NSCs revealed a mild and transient increase followed by a strong decrease of the heavy polysomal fractions, as compared to untreated controls (Figure 2A,B). Despite this IFN-β´s biphasic control of global translation, gene set enrichment analysis of Ribo-Seq identified specific subsets of transcripts exhibiting either a steady enhanced or repressed translation (translation efficiency; TE) (Figure 2C,D; S2A,B). mRNAs encoding DNA replication and cell cycle-related proteins were steadily repressed, in agreement with the detected arrest in G_0. Conversely, interferon stimulated genes (ISGs), crucial components of the antiviral response (Mazewski et al., 2020), exhibited a gradual increase of TE. This enhanced translation was confirmed by RT-qPCR of the polysomal fractions for a subset of ISGs including *Ifit3* and *Irf9* (Figure S2C). Notably, IFN-mediated translation of ISGs had always been linked to upregulation of cap-dependent translation (Kroczynska, Mehrotra, Arslan, Kaur, & Platanias, 2014; Mazewski et al., 2020). How translation of ISGs is maintained despite a global downregulation of translation remains unclear.

mTOR contributes to the IFN-induced biphasic control of mRNA translation

To dissect the molecular drivers of the IFN-induced biphasic control of mRNA translation, we examined mTOR involvement. mTOR is a key checkpoint in the control of metabolic pathways, including regulation of cap-dependent translation (G. Y. Liu & Sabatini, 2020). Type I, II and III IFNs have been reported to activate the PI3K/mTOR pathway in different cell types (Ivashkiv & Donlin, 2014; Lekmine et al., 2004, 2003; Syedbasha et al., 2020). There are also recent reports on mTOR inhibition by IFN-β and IFN-γ (X. Su et al., 2015; Vigo et al., 2019). To assess the impact of mTOR in the observed IFN-β´s biphasic control of global translation in NSCs, we inspected the TE of mRNAs containing the 5' terminal oligopyrimidine (TOP) motif, referred to as TOP-mRNAs (Avni, Biberman, & Meyuhas, 1996). Translation of TOP-mRNAs is susceptible to mTOR activity (Thoreen et al., 2012), which makes it a faithful readout of mTOR activity. We observed that IFN-β controlled TOP-mRNAs in a biphasic

manner, reproducing the early mild up- and late drastic down-regulation of translation (Figure 2E,F; S2D). Further inspection of the Ribo-Seq profiles of expressed TOP-mRNAs confirmed this biphasic regulation with a differential abundance of footprints in their coding sequence (CDS) upon IFN-β treatment (Figure 2G,H). We next examined the phosphorylation state of mTOR pathway components. The same biphasic regulation of phosphorylation was observed in the downstream substrates of mTOR, ribosomal protein S6 kinase (S6K), ribosomal protein S6 (S6) and eIF4E-binding protein (4E-BP) (Figure 2I). In particular, Thr389 phosphorylation of S6K, a direct target of mTORC1 (Ma & Blenis, 2009), confirmed the specific modulation of mTORC1 by IFN-β in NSCs.

Biphasic regulation of mRNA translation by IFN-β involves mTORC1 and p-eIF2α

We next set out to address the molecular underpinnings of mTOR biphasic modulation. The control of mTOR by type I IFN in different cell models mainly relies on the crosstalk of the IFN-activated JAK/STAT pathway with the PI3K pathway (Mazewski et al., 2020; Platanias, 2005). In this scenario, IFN activates JAK1/TYK2 kinases that interact with the insulin receptor substrate 1 (Irs1), which modulates the activity of the PI3K-pathway components Akt and TSC1/2(Kim & Guan, 2019; Platanias, 2005). Notably, we found that upon IFN-β treatment, phosphorylation of Akt^{Thr308} and $TSC2^{Thr1462}$ not only increased, but followed a biphasic mode of regulation (Figure 3A) as for mTORC1 (Figure 2). While the early mTORC1 upregulation arises from the crosstalk between IFN-β and PI3K, additional mechanisms are necessary to explain the late downregulation of the PI3K pathway, as recently hypothesized (Muendlein et al., 2020). Hyperactivation of mTORC1 can trigger negative feedback loops involving mTORC2 and Irs1/2, that reverse the initial IFN-β-mediated PI3K-Akt activation (Hsu et al., 2011; Rozengurt, Soares, & Sinnet-Smith, 2014) (Figure 3B). To be able to follow kinase activities downstream of IFN-β in a broader manner, we acquired the proteomic and phospho-proteomic profiles of NSCs treated with IFN-β or vehicle at 2h and 14h. Analysis of these profiles revealed a downregulation of p-Akt^{Ser473}, an mTORC2-dependent site (Sarbassov, Guertin, Ali, & Sabatini, 2005), only after long exposure to IFN-β (Table S1). Moreover, the early upregulation of the activity read-out of IRS1 (Esposito, Li, Cama, & Quon, 2001), p-$Irs1^{Tyr608}$, faded upon long exposure to IFN-β. Additionally, p-$Irs1^{Ser1134}$ and p-

Irs1^{Ser1137} displayed the biphasic trend, correlating with the activation status of mTOR (Copps & White, 2012; Karlsson et al., 2021; Langlais et al., 2011). This suggests that prolonged IFN-β exposure induces negative feedbacks converging on Akt that inhibits mTORC1 in NSCs. Akt regulates mTORC1 through inactivation of the negative regulator of mTORC1, TSC1/2 (Kim & Guan, 2019). According to our results, the two temporal components of the biphasic regulation of mTOR by IFN-β rely on TSC1/2. To validate this, we generated heterozygous TSC2 mutant NSC clones by CRISPR/Cas9 (TSC2^{mut}). NSCs where CRISPR/Cas9 did not reduce TSC2 protein levels were treated as control (TSC2^{ctrl}) to exclude off-target or manipulation-derived artefacts (Figure S3A). TSC2^{mut} NSC clones had a basally increased mTOR activity and displayed a milder inhibition of global translation in response to IFN-β (Figure S3B,C). As hypothesized, the biphasic regulation of mTORC1 activity, as measured by p-S6K^{Thr389}, was strongly blunted in TSC2^{mut} NSCs (Figure S3D).

Along with the inhibitory feedback loops, transcriptionally upregulated ISGs, such as PKR, promote a delayed inhibition of global mRNA translation (Ivashkiv & Donlin, 2014). PKR (*Eif2ak2*) is activated by dsRNA and phosphorylates the translation factor eIF2α at Ser51, resulting in a global inhibition of mRNA translation initiation (Gal-Ben-Ari, Barrera, Ehrlich, & Rosenblum, 2019). We found that extended exposure to IFN-β increased PKR protein levels and phosphorylation in poorly-described residues (Piazzi, Bavelloni, Faenza, & Blalock, 2020) (Figure S3E; Table S1). Of note, NSCs exposed to IFN-β induced an increase in p-eIF2α^{Ser51}, which intensify the inhibition of mRNA translation already exerted by late inhibition of mTORC1 (Figure 3C). Furthermore, activated PKR can inhibit Irs1(Nakamura et al., 2010), contributing to the mTORC1 feedback inhibitory loops. In addition to the regulation of global mRNA translation, p-eIF2α^{Ser51} is associated with the alternative use of upstream open reading frames (uORFs) located in the 5' untranslated region (5'UTR)(Young & Wek, 2016). IFN-β increased local 5'UTR footprint density in a subset of genes while maintaining unaltered levels in the CDS, indicating alternative uORF usage (Figure 3D). Consistently, while translation upregulation in the CDS shifted mRNAs to heavy polysomes, a higher ribosomal density in uORFs shifted the associated mRNAs into light polysomes (Figure S3F).

Initial uncoupling of TOR and cell cycle by IFN-β

It did not remain unnoticed that the IFN-induced transient increase of mRNA translation coincides in time with the gradual inhibition of cell cycle in NSCs. We therefore assessed how the IFN type I response uncouples translation and cell cycle in NSCs. Given that NSCs remained significantly longer in G_1 upon IFN-β treatment (Figure 1D), we hypothesized that IFN could trigger the inhibition of G_1/S checkpoint regulators Cdk4/6. These kinases have recently emerged as a dual regulator of cell growth and proliferation via TSC2 and modulators of proliferation of NSCs and neurogenic progenitors in the adult brain (Artegiani, Lindemann, & Calegari, 2011; Lange, Huttner, & Calegari, 2009; Romero-Pozuelo, Figlia, Kaya, Martin-Villalba, & Teleman, 2020). Cdk4/6 control the G1/S transition by phosphorylation of Rb1 and consequent expression of S-phase genes (Topacio et al., 2019). We found that IFN-β reduced p-Rb^{Ser780}, a Cdk4/6-dependent phosphosite, in a progressive manner in NSCs *in-vitro* (Figure 3E). Moreover, IFN-β treatment led to the phosphorylation of the regulatory partner of Cdk4/6, CyclinD1 at Thr286 (Table S1), a phosphosite involved in cytoplasmic translocation and degradation of CyclinD1(Guo et al., 2005). We believe that the early activation of PI3K-Akt masks a yet weak inhibition of Cdk4/6 that is later reversed by a stronger inhibition of Cdk4/6 and the late mTORC1 inhibitory feedback loops (Figure 3F).

IFN-β represses *Sox2* translation via its 5' pyrimidine rich motif through the biphasic control of mTOR

A dual regulation of mTOR and cell cycle is needed to repress translation of *Sox2* and allows transition out of an activated stem cell state into a differentiated neuroblast (Baser et al., 2019). Sox2 levels are likewise reduced in quiescent NSCs to avoid replicative stress (Marqués-Torrejón et al., 2013). We therefore wondered whether the orchestration of TOR and cell cycle by IFN type I would also lead to posttranscriptional repression of *Sox2* expression. Interestingly, *Sox2* remained oblivious to the initial increase of mTORC1 activity and even exhibited a subtle repression at 2h after IFN-β, differently to TOP-mRNAs (Figure 3G; S2D). Indeed, *Sox2* translation was strongly repressed in NSCs following long exposure to IFN-β (Figure 3G). Since IFN-β-mediated repression was much stronger than the one we previously measured following TOR inhibition and cell cycle arrest (Baser et al., 2019), we wondered

whether the early decoupling of growth and proliferation exerted by IFN-β would be required to more effectively repress *Sox2* translation. In order to evaluate this hypothesis, we blocked the early mTOR activation with Torin1 in IFN-β-treated NSCs. To examine the involvement of the 5'UTR of *Sox2* in this repression, we established a luciferase assay in which we cloned the 5'UTR region of *Sox2* as well as of the TOP-containing mRNA *Rps21* upstream of the *Renilla* luciferase CDS (Figure 3H). Torin1 treatment alone effectively repressed translation of the TOP-mRNA *Rps21* but failed to repress *Sox2* (Figure S3G), in agreement with previous findings (Baser et al., 2019). IFN-β treatment alone also effectively repressed Sox2 (Figure 3I). However, IFN-β repression of *Sox2* was prevented by Torin1 (Figure 3I). This highlights the importance of a biphasic control of mRNA translation by IFN-β in stem cells and points to the fact that dual inhibition of mTOR and cell cycle is not sufficient to completely suppress translation of *Sox2*. In addition, we recently proposed that a pyrimidine rich motif (PRM) present in the 5' UTR of relevant stem genes like *Sox2* and *Pax6* could be responsible for posttranscriptional repression of factors involved in stem cell exit (Baser et al., 2019). PRM is present in different mRNAs downregulated at the onset of differentiation such as *Sox2* and *Pax6* and can co-localize with the TOP motif as in the case of *Rps21* (Baser et al., 2019). To evaluate the contribution of the PRM to the repression of *Sox2*, we mutated the PRM using *Rps21* as control (Figure 3H). The deletion of the PRM attenuated the repression of *Sox2* exerted by IFN-β in NSCs (Figure 3J) and did not affect expression of the PRM-mutated *Rps21*, driven by the prevalent TOP motif.

Extrinsic interferons act on neural stem cells and fine-tunes progenitor production across all ages

Altogether we have shown that IFNs regulate NSC dynamics in addition to their reported antiviral function in stem cells. The antiviral-related ISGs are transcribed in an interferon-independent manner and shut down upon differentiation *in vitro* (Wu et al., 2018).To examine if this is also the case for ISGs involved in regulating stem cell dynamics, we profiled the expression of ISGs in NSCs and their progeny in the natural environment of the brain. For this, we profiled the transcriptomes of individual vSVZ-NSCs, their progeny (Tlx-mediated eYFP$^+$ cells) and some neighboring cells from WT and IFNAGR KO mice at young and old ages (Figure 4A). scRNAseq analysis using previously defined markers (Kalamakis et al., 2019; Llorens-Bobadilla et al., 2015)

identified quiescent NSC (qNSC) 1 and 2, active NSC (aNSC), trans-amplifying progenitors (TAPs) and neuroblasts (NBs) (Figure 4B; S4A). We found expression of type I IFN receptors in all cell types along the lineage (Figure S4B), in addition to the recently reported expression of type II IFN receptors (Dulken et al., 2019). To score the interferon response in these cells, we developed a "NSC Type I interferon response" signature consisting of the most transcriptionally upregulated genes from the Ribo-Seq of NSCs treated with IFN-β (Figure 4C; S4C). In addition, we scored relevant interferon- and inflammation-related gene sets from MSigDB (Figure S4D). First, we confirmed the previously reported upregulation of type I ISGs (Kalamakis et al., 2019), but also of the antiviral-related ISGs (Wu et al., 2018) "Wu et al., (2018)" with age in WT NSCs (Figure 4C). Notably, ISG-expression is shut down in the progeny and not affected by age, indicating that the progeny is protected from age-related inflammation. Once maturation is completed this protection vanishes and neurons exhibit a similar ISG expression as stem cells that is similarly affected by age. Excitingly, in the absence of IFN receptors, while the levels of ISGs are slightly higher, they are not any more influenced by age (Figure 4C, right panel). This indicates that stem cell regulation by ISGs involves extrinsic regulation by interferons. This extrinsic regulation is also relevant for regulation of ISGs in endothelial cells, while ISG expression in microglia increases with age but remains largely unaffected by the loss of IFN receptors (Figure 4C, right panel).

Given the relevance of extrinsic IFNs for NSCs and aging, we further explored its potential role as a therapeutic target. In our models, we know that the activation rate of NSCs directly influences the production of progenitors. Young IFNAGR KO mice have a lower activation rate of NSCs than WT, suggesting a decreased productivity. Older IFNAGR KO mice however have a higher activation rate than control counterparts, suggesting increased productivity (Figure 1C). This response suggests a possibility for improving progenitor production in WT animals by selecting an optimal time point to block IFN function. To investigate this, we simulated a modified model with IFN-dependent switches in model parameters at arbitrary time points (Supplementary Data). The intervention was modelled by switching the activation rate and self-renewal parameters estimated from WT mice to the functions estimated for IFNAGR KO mice. This best mimic an acute clinical intervention for systemic neutralization of interferons. Interventions simulated at young ages resulted in a significant loss of NSCs, dropping from thousands to hundreds in the short term

(Figure 4D). However, this effect diminished with time resulting in similar cell counts in old age (Figure 4D; S4E). Since total NSCs are not necessarily indicative of proper functioning, we also computed the cell flux from aNSC to progenitors (progenitor production). Simulations of young age interventions showed drastically reduced progenitor production on a short time scale, which ultimately changed to an increased progenitor production in old ages (Figure 4E). Interventions in older mice (after ~300 days) showed to always be beneficial. We next compared the summary effect of an intervention in terms of the life-long progenitor production. The interventions at young ages had diminished progenitor production when compared to WT, while the maximal benefit of the life-long production was achieved by intervention at about 350 days of age (Figure 4E; S4F). Curiously, this was also the age at which the activation rate for WT dropped below the constant IFNAGR KO activation rate (Figure 1B). Overall, this shows that there may be benefits to progenitor production from blocking interferon response at increasing ages, while it may have strong adverse effects on short-term productivity and stem cell counts when done too early. In agreement with our predictions, local blockade of CXCL10 signaling in the aged brain increased progenitor production from vSVZ-NSCs (Blank et al., 2016; Kalamakis et al., 2019). CXCL10 is induced in endothelial cells upon systemic IFN-β, which itself is not able to cross the blood brain barrier (Blank & Prinz, 2017). Last, this and the previous reported neutralization of IFN (Baruch et al. 2014), would also suggest that a late intervention blocking IFN signaling is beneficial despite the recently reported IFN memory in stem cells (Haas et al., 2017).

Discussion

Interferons are bona fide regulators of stem cell homeostasis and potential targets to repair the aging brain

Stem cells exhibit an intrinsic IFN signature, i.e., constitutive expression of ISGs independent of interferon receptor stimulation, which is unique to stem cells and protects them against viral infections (Wu et al., 2018). In addition, Wu et al., also reported that stem cells are refractory to extrinsic IFNs. Our study shows that in the natural environment of the brain, ISG expression is highest in NSCs but also present, albeit to a lower extent, in fully differentiated newborn neurons. It is however the intermediate maturation stages where ISG expression disappears. Notably, aging increases ISG expression in stem cells and mature newborn neurons, but not in these

intermediate stages. We show that this age-dependent increase relies on expression of IFN receptors, indicating that neural stem cells are indeed responsive to interferons both *in-vivo* and *in-vitro* as it is the case for their differentiated counterparts. At the same time, intermediate progenitor stages are shown to be refractory to extrinsic interferon and probably represent the most susceptible cells to viral infection along the neurogenic lineage. Hence, the high number of intermediate progenitors during development could contribute to viral infections being a life-threatening risk at this age. Strikingly, our data-informed modeling predicts that blocking signaling of IFN in the adult brain lead to beneficial higher production of neurons, while an early intervention can be detrimental for the individual.

Type I IFN induces stem cell quiescence by a biphasic control of mRNA translation and cell cycle exit

IFNs modulate stem cells across different tissues but the molecular underpinnings of this regulations are yet poorly described (Demerdash, Kain, Essers, & King, 2021; Hou, Huang, Ayansola, Masatoshi, & Zhang, 2021; Kalamakis et al., 2019; Zhang et al., 2020). Performing polysome profiles and ribosome footprinting on IFN-β treated NSCs we find that IFN-β induces a biphasic control of mRNA translation. This regulation involves a transient activation of mTORC1 followed by its inhibition, as opposed to the previously reported unidirectional modulation of mTOR by type I IFN (Mazewski et al., 2020). Future studies should address whether this response takes place across different tissues and whether this is a hallmark of stem cells. We further show that this transient activation of mTOR is the result of the crosstalk between IFN-β signaling and PI3K. The resulting late inhibitory feedback loops acting on Akt and the activation of PKR together with phosphorylation of eIF2α, ultimately lead to the late and profound inhibition of mRNA translation. Notably, our data suggests that IFN-β treatment in NSCs not only induces the expression but also activates PKR in a dsRNA-independent manner. This is an undescribed feature of IFNs in stem cells as a similar response has only been reported in an interferon-selected carcinoma line harboring oncogenic mutations (Q. Su et al., 2007). As a whole, these pathways converge in a profound shut down of translation that keeps NSCs dormant. High levels of p-eIF2α are also associated to self-renewal and quiescence induction in embryonic and adult stem cells (Friend, Brooks, Propson, Thomson, & Kimble, 2015; Zismanov et al.,

2016). Similarly, chronic IFN type I promotes quiescence after a transient activation of hematopoietic stem cells (Pietras et al., 2014).

Accordingly, we find that IFN-β shifts NSCs to a quiescent G_0 state, as opposed to the previously reported increase in cell-cycle length in quiescent NSCs (Daynac, Morizur, Chicheportiche, Mouthon, & Boussin, 2016). Remarkably, inhibition of Cdk4/6 upon IFN-β treatment transiently uncouples growth and proliferation in NSCs. A similar uncoupling of proliferation and protein synthesis was observed upon differentiation of skin stem cells, but the drivers of this response remained elusive (Blanco et al., 2016). Of note, senescent cells, a hallmark of aging (Fulop et al., 2018; Zhu et al., 2021), steadily uncouple translation and cell cycle (Payea, Anerillas, Tharakan, & Gorospe, 2021). Differently to NSCs, a late coupling of translation and cell cycle has not been described in senescence. Intriguingly, IFN-β is one of the main drivers of senescence. Cytosolic chromatin fragments present in senescent cells activate cyclic GMP-AMP synthase (cGAS) that, in turn, triggers the production of inflammatory factors including IFN-β, thereby inducing paracrine senescence (Glück & Ablasser, 2019). Although the prevalence of senescent cells increases with age in the neurogenic niches in the brain (Fernández-Fernández et al., 2012; Jin et al., 2021; Molofsky et al., 2006; Ogrodnik et al., 2019), how NSCs are protected from senescence remains unknown. Overall, our study highlights a previously undescribed feature of the IFN-β response in stem cells.

Type I IFN induces a biphasic control of mTOR that represses *Sox2* translation in NSCs

We recently reported that a dual regulation of mTOR and cell cycle is needed to repress translation of *Sox2* in NSCs (Baser et al., 2019). We now identify IFN type I as a regulator of this response. Furthermore, we narrow down the nature of this repression to the transient activation of TOR and the presence of the recently described pyrimidine-rich motif (PRM) present on *Sox2*'s 5'UTR (Baser et al., 2019). In this study, we addressed the role of repression of *Sox2* translation in the transition of an activated stem cell into a differentiated neuroblast (Baser et al., 2019). Sox2 levels are likewise reduced in quiescent NSCs to avoid replicative stress (Marqués-Torrejón et al., 2013). The determinants of directionality into a differentiated progenitor or a quiescent stem cell state following repression of Sox2 remain subject of future studies. Notably, Sox2 expression is reduced in the aging brain, correlating with increased quiescence in NSCs (Carrasco-Garcia et al., 2019).

Collectively, our findings unveil interferons as *bona fide* regulators of stem cell function during tissue homeostasis as well as in aging. Mechanistically, IFN-β arrests NSCs at G_0 of the cell cycle and drives a transient TOR activation followed by a profound decrease of TOR activity and global protein synthesis. This biphasic regulation is orchestrated by mTORC1, PKR and p-eIF2α. In addition, we show that the transient increase of TOR activity is required for post-transcriptional repression of PRM-containing transcripts, such as *Sox2*, that contribute to the exit from the activation state in stem cells (Figure 4F). Future studies should unveil the potential uniqueness of this biphasic response in stem cells across different tissues and its relevance for the prevention of senescence in stem cells. Our study indicates that IFN's control of the activation rate and self-renewal of NSCs adapts the output of differentiated progenitors to demand. In young brains, with high demand, interferon would increase the output, and vice versa, decrease the number of generated progenitors in the less active aging brain. Therefore, while the loss of IFN signaling is beneficial in the old brain, it is detrimental in young individuals. The fact that levels of ISG expression in the aging brain are regulated by IFN ligands, discloses IFNs as potential therapeutic target to improve stem cell homeostasis and repair in the aging brain.

Acknowledgments

We thank S. Wolf & D. Helm from the DKFZ Genomics and Proteomics Core Facility; S. Schmitt from the DKFZ Flow Cytometry Core Facility; J.-P. Mallm from the DKFZ scOpenLab; the DKFZ Centre for Preclinical Research; K. Volk, K. Menzner & H. Abendroth for technical assistance; B. Bukau and the members of the Martin-Villalba laboratory for critical comments.
This work was supported by the European Research Council (ERC; REBUILD_CNS), the Helmholtz Zukunftsthema Aging and Metabolic Programming (AMPro) ZT-0026, the German Research Foundation (DFG; SFB873), and the German Cancer Research Center (DKFZ).

Author's contributions

Conceptualization, A.M.-V., A.M.-C., D.C-I., M.S. and J.H.; Methodology, M.S., D.C-I. and S.C.; Investigation, M.S., D.C-I., S.C. and M.Z.; Software & Formal Analysis, J.H. and M.G.; Data Curation, J.H.; Visualization, J.H., D.C.I., M.S. and M.G.; Resources, M.B., G.K., A.J. and T.H. Writing – Original Draft, D.C.-I., A.M.-V., A.M.-C. and J.H.; Writing – Review & Editing, D.C.-I.; Supervision, A.M.-V., A.M.-C., A.T. and S.A.; Project Administration & Funding Acquisition, A.M.-V.

Declaration of interests

The authors declare no competing interests.

Figures

Figure 1

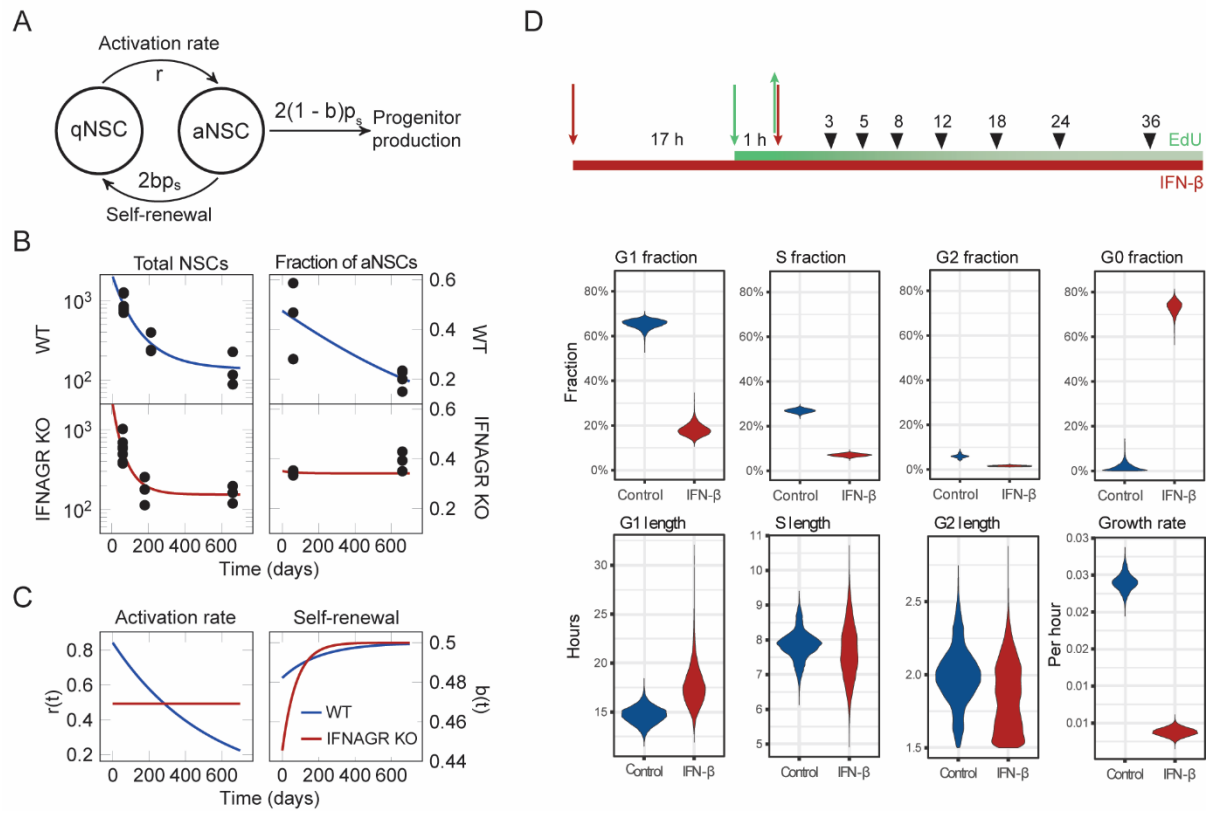

Figure 1. Interferon regulates stemness at all ages and halts NSCs in G_0
(A) Graphical depiction of mathematical model describing the activation (at rate r) of quiescent neural stem cells (qNSC) into active NSC (aNSC) followed by their progression (at rate p_s) into either two downstream progenitors (at probability 1−b) or two NSCs (at probability b) that return to quiescence. In models with time-dependent parameters, $b \equiv b(t)$ and $r \equiv r(t)$, See Supplementary Data 1 for details.
(B) vSVZ niche FACS quantifications of total NSCs (Total NSCs) & immunofluorescence quantification of aNSCs (Fraction of aNSCs) in WT or IFNAGR KO mice at 2, 7 and 22 months old (MO). Data from individual mice is plotted. Inferred dynamics are depicted as a blue (WT) or red (IFNAGR KO) line over time. n = 3-8.
(C) Inferred parameters are depicted as a blue (WT) or red (IFNAGR KO) line over time.
(D) CycleFlow experimental scheme (upper panel) and inferred cell cycle fractions as well as properties (lower panels) in IFN-β-treated NSCs. See also Figure S1. n = 3.

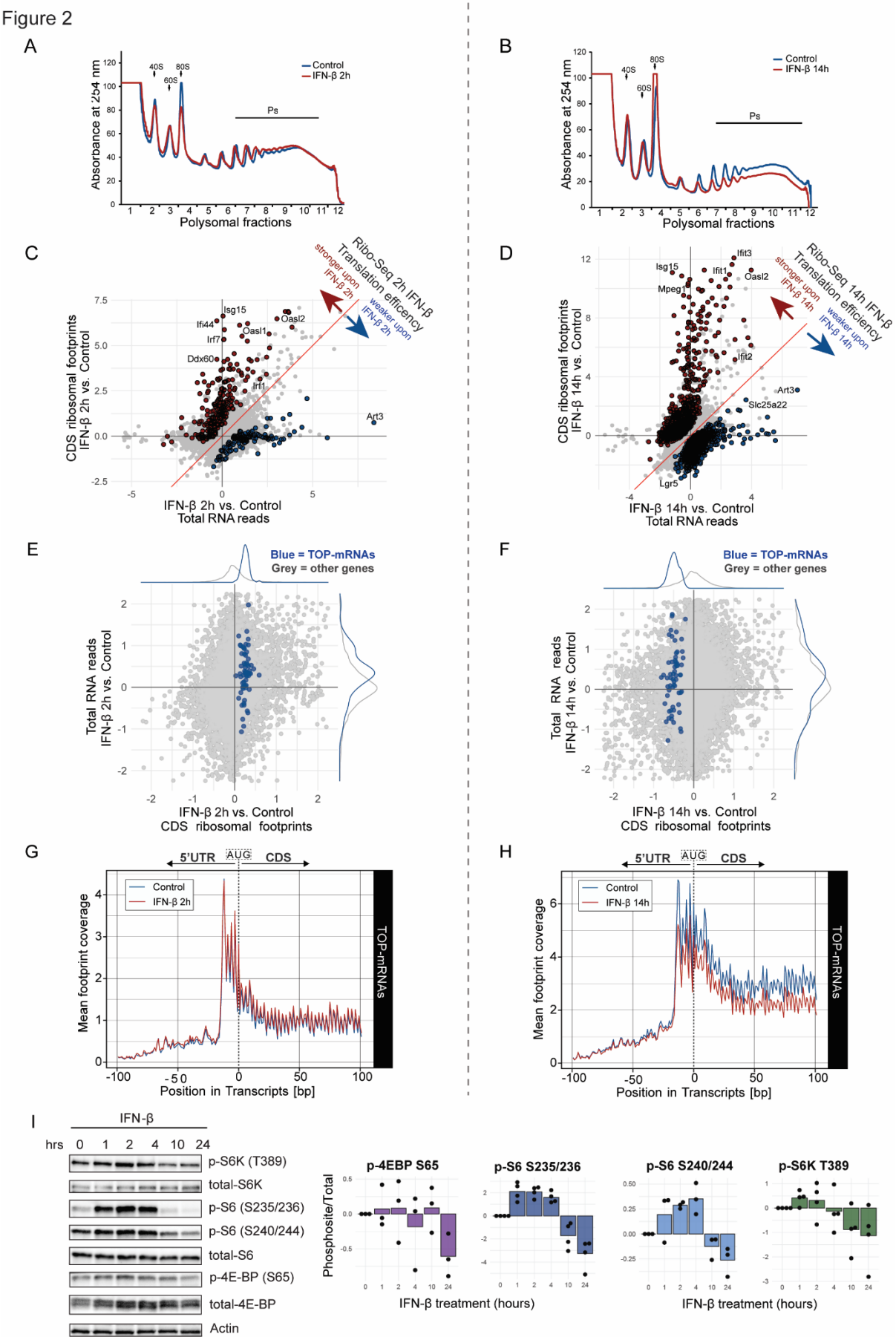

Figure 2. IFN-β controls mTORC1 shaping a biphasic regulation of mRNA translation in NSCs

(A & B) Representative polysome profiles of NSCs treated with IFN-β for 2h and 14h treatment. Arrows indicate the 40S, 60S and 80S subunits of the ribosome.
(C & D) Results of Ribo-Seq depicting translation efficiency as the interaction of log2 fold changes (LFC) between footprints (ribosome protected reads) and total RNA at 2h and 14h IFN-β treatment. FDR < 10%, LR-Test. Genes with a p value<0.1 after FDR correction are highlighted. For associated GO terms see also Figure S2. n = 3.
(E & F) Ribo-Seq results of 2h and 14h IFN-β treatments. Footprints mapped to the CDS are referred to as "CDS counts". 5' terminal oligopyrimidine motif-containing mRNAs (TOP-mRNAs) highlighted in blue. n = 3.
(G & H) Coverage profile of ribosome-protected reads (footprints) of TOP-mRNAs in 2h and 14h IFN-β treatment. Nucleotide 0 depicts the start codon (AUG) marking the interface between 5' untranslated region (5' UTR) and coding sequence (CDS).
(I) Representative WB and phosphorylation levels quantification (log2FC) of the mTOR-related proteins ribosomal protein S6 kinase (S6K), ribosomal protein S6 (S6) and eIF4E-binding protein (4E-BP) from NSCs treated with IFN-β and normalized to control (t=0h). Bars represent the mean value. n = 3-4.

Figure 3

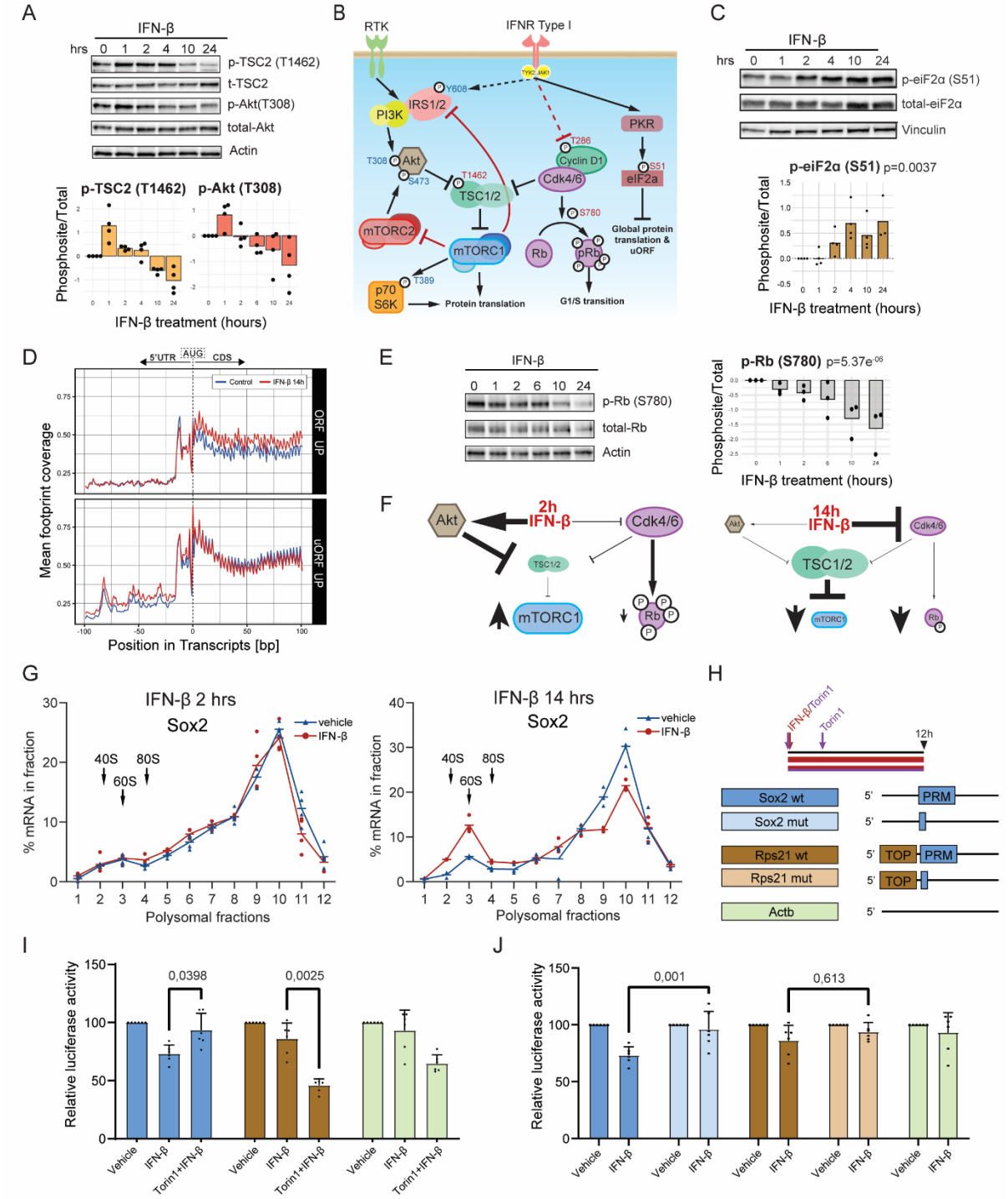

Figure 3. IFN-β's biphasic control of mTORC1 uncouples growth and cell cycle and represses Sox2 translation via its 5' PRM motif

(A) Representative WB image and quantification (log2FC) of p-TSC2^{Thr1462} & p-Akt^{Thr308} from IFNβ-treated NSCs normalized to control (t=0h). Bars represent the mean value. n = 4.

(B) Schematic representation of the interferon type-I signaling pathway and its crosstalk with the receptor tyrosine kinase (RTK) pathway. Activatory (blue) and inhibitory (red) phosphosites are depicted.

(C) Representative WB images and quantifications (log2FC) of p-eIF2α^{S51} in IFN-β-treated NSCs normalized to control (t=0h). See also Figure S3. Bars represent the mean value. n = 3. Spearman's rank correlation test. p ≡ p-value.

(D) Coverage profile of ribosome-protected reads (footprints) in genes with upregulated canonical (upper) or alternative upstream (lower) ORFs upon extended IFN-β treatment. Nucleotide 0 depicts the

start codon (AUG) marking the interface between 5' untranslated region (5' UTR) and coding sequence (CDS).
(E) Representative WB image and quantifications (log2FC) of p-Rb1^{Ser780} from IFN-β-treated NSCs normalized to control (t=0h). Bars represent the mean value. n = 3. Spearman's rank correlation test. p ≡ p-value.
(F) Schematic representation of the prevailing signaling pathways driving the early inhibition and late activation of mTORC1.
(G) Polysome profiling (RT-qPCR) of Sox2 mRNA upon 2h and 14h IFN-β treatment. Hyphens represent mean of biological replicates. Arrows represent the 40S, 60S and 80S subunits of the ribosome. n = 3-4.
(H) Experimental layout of IFN and Torin1 treatments (upper panel). Schematic representation (lower panel) of the 5'UTR constructs priming the *renilla* luciferase. TOP = 5'Terminal Oligopyrimidine motif; PRM = 5' Pyrimidine Rich Motif.
(I & J) Luciferase activity controlled by the upstream 5'UTR fragment from *Sox2* (WT and mutant), *Rps21* (WT and mutant) and *Actb*. Data is normalized to vehicle and is represented as mean ± SD. n = 6. Two-way ANOVA with Tukey's multiple comparisons test (p-value specified).

Figure 4

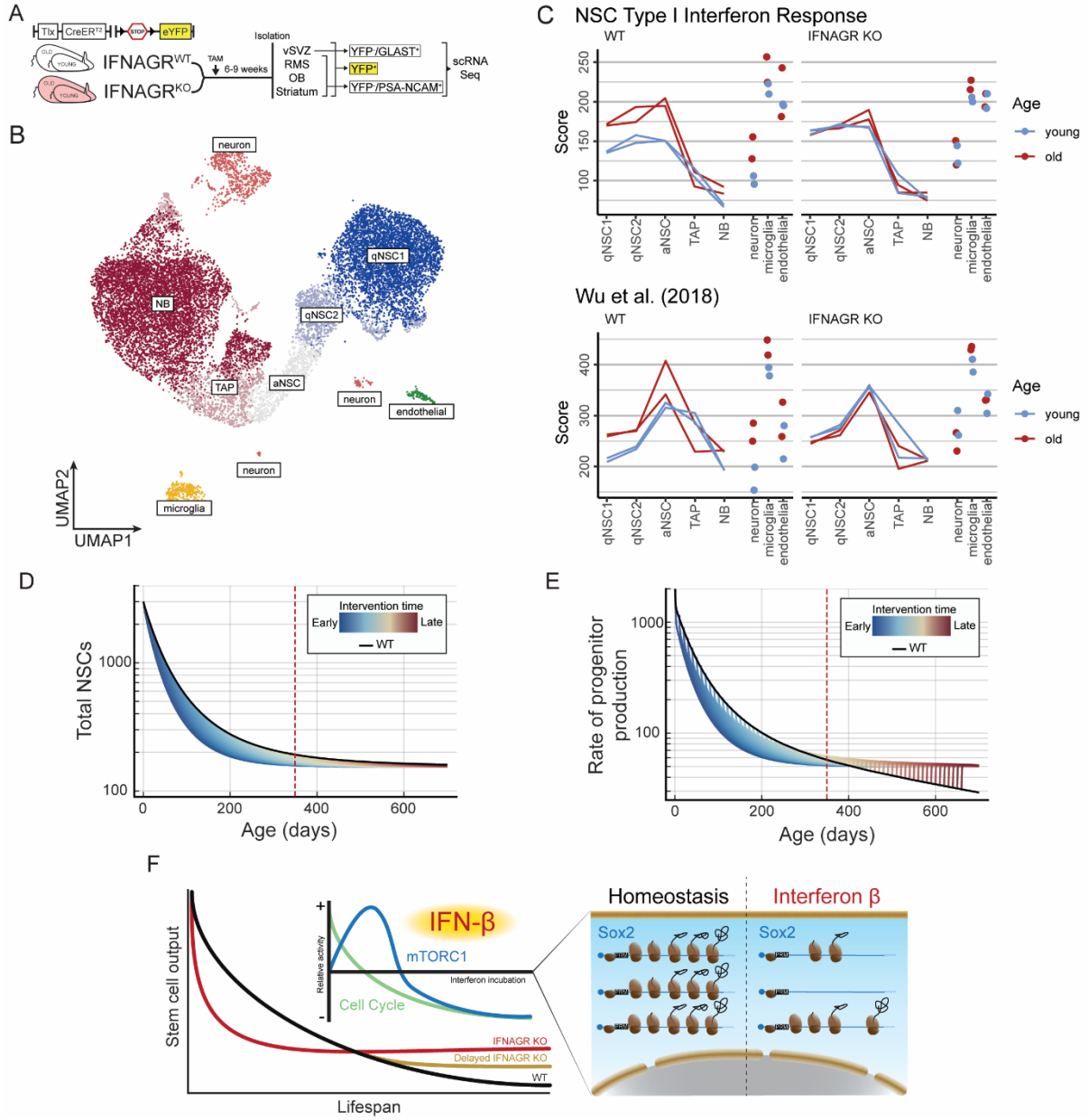

Figure 4. Extrinsic interferons act on neural stem cells and fine-tunes progenitor production across all ages

(A) Experimental layout for scRNA-Seq in young and old mice lacking interferon receptors. All mice represent TiCY (Tlx reporter, see methods) that are either IFNAGR WT or KO. vSVZ (Ventricular Subventricular Zone), RMS (Rostral Migratory Stream), OB (Olfactory Bulb), TAM (Tamoxifen).

(B) UMAP embedding showing the single cells in this analysis with their cell types. See also Figure S4. n = 2 biological replicates per age and genotype.

(C) Scores derived for the different gene signatures (bulk stem cell-derived "NSC Type I Interferon Response" and "Wu et al. (2018)" from Wu et al. (2018)) and cell types in our analysis at varying ages in wildtype (WT) and IFNAGR KO cells. n = 2 biological replicates per age and genotype.

(D) Induced interferon knockout simulations (colored, each color represents a different intervention timepoint) against wildtype simulations (black) showing the total number of stem cells across age. Dashed red line denotes age 350 days.

(E) The rate at which progenitors are produced $(2\, p_s\, (1-b)\, aNSC)$ from NSCs for induced interferon knockout simulations with interferon dependent self-renewal (coloured, each colour represents a different intervention timepoint) and WT simulations (black). Dashed red line denotes age 350 days.

(F) Graphical abstract.

Methods

RESOURCE AVAILABILITY

Further information and requests for resources and reagents should be should be directed to and will be fulfilled by the Lead Contact, Ana Martin-Villalba (a.martin-villalba@dkfz-heidelberg.de). Some materials may require execution of an MTA.

Data and code availability

Raw Single-cell RNA-seq and Ribo-Seq data have been deposited at the Gene Expression Omnibus (GEO) and are publicly available as of the date of publication. Accession numbers will be listed in the key resources table when available. Original western blot images will be deposited at Mendeley and will be publicly available as of the date of publication. The DOI will be listed in the key resources table.
All original code will be deposited at https://github.com/Martin-Villalba-lab/Data/ and publicly available as of the date of publication.
Any additional information required to reanalyze the data reported in this paper is available
from the lead contact upon request.

EXPERIMENTAL MODEL AND SUBJECT DETAILS

Mice

C57BL/6 male mice were purchased from Janvier or bred in-house at the DKFZ Center for Preclinical Research. Male IFNAGRKO (Huang et al., 1993; Müller et al., 1994) (IFNAR$^{-/-}$IFNGR$^{-/-}$) were backcrossed to a C57BL6 background. Male TiCY mice (Tlx-CreERT2-YFP)(H. K. Liu et al., 2008) (TiCY [B6-Tg(Nr2e1-Cre/ERT2)1GscGt(ROSA)26Sortm1(EYFP)CosFastm1Cgn/Amv]) were crossed with IFNAGRKO mice to generate TiCY-IFNAGRKO mice ([B6-Tg(Nr2e1-Cre/ERT2)1Gsc Gt(ROSA)26Sortm1(EYFP)CosFastm1CgnIfnar1tm1AgtIfngr1tmAgt/Amv]). Animals were housed under standard conditions and fed ad libitum. All procedures were approved by the Regierungpräsidium Karlsruhe.

METHOD DETAILS

Cell culture and treatments

For NSC isolation, the subventricular zones from 8-12 weeks old male C57BL/6 mice were isolated as described (Mirzadeh, Doetsch, Sawamoto, Wichterle, & Alvarez-Buylla, 2010). The tissue was dissociated using the Neural Tissue Dissociation Kit with Papain (Miltenyi Biotec) following the manufacturer's instructions. Cells were cultured in Neurobasal A Medium supplemented with 2% B27 Supplement serum-free, 1% L-Glutamine (all from ThermoFisher), 2 µg/ml of heparin, 20 ng/ml of human basic FGF (ReliaTech) and 20 ng/ml of human EGF (Promokine). Cells were maintained in a 37°C, 5% CO_2 incubator.
For the treatment with interferon, mouse recombinant IFN-β (Millipore) diluted in DPBS with 0.1% Bovine serum albumin BSA (Roche) were added directly to the culture media at final concentration of 40 u/ml for the indicated time. Control cells were treated with the same volume of 0.1% BSA in PBS.
For the treatment with Torin1 (Cayman Chemical), Torin1 was dissolved in 100% DMSO and added to cells at 250 nM for the indicated time. Control cells were treated with the same volume of DMSO.

CRISPR-mediated generation of TSC2$^{+/-}$ NSCs

CRISPR-Cas9 gRNAs targeting exon 2 of *Tsc2* (ENSMUSG00000002496) were designed using the CCTop target online predictor (Stemmer, Thumberger, Del Sol Keyer, Wittbrodt, & Mateo, 2015) and cutting efficiency was evaluated by T7EI Assay using T7 Endonuclease I (NEB). We selected the TSC2Ex2-gRNA (TGTTGGGATTGGGAACATCGAGG) and cloned it into the Cas9-containing plasmid pSpCas9(BB)-2A-GFP (Addgene) as described (Ran et al., 2013) (see Table S1).
For nucleofection, 1 x 10^6 NSCs were mixed with 2.5 µg of corresponding DNA using Amaxa P4 Primary Cell 4D-Nucleofector X Kit S (Lonza) with CA137 programme in a 4D-Nucleofector X Unit (Lonza). Cells were incubated for 24 hours at 37°C and 5% CO_2. GFP-positive single NSCs were FACS-sorted into 96-well plates. Single NSC colonies were expanded and TSC2 abundancy was checked by western blot (see section below).

Flow cytometry analysis

For the flow cytometry analysis, vSVZ single cell suspensions from mice at the specified ages were generated and stained for flow cytometry analysis as described (Llorens-Bobadilla et al., 2015). Briefly, vSVZ was microdissected using the Neural Tissue Dissociation kit with Trypsin and Gentle MACS dissociator (Miltenyi). Cells were stained with the following antibodies: O4 APC-Cy7 (1:100), GLAST (ACSA-1)-PE (1:50) (all from Miltenyi), Ter119 APC-Cy7 (Biolegend; 1:100), CD45 APC-Cy7 (BD; 1:200), Prominin1-APC (eBioscience; 1:75), Alexa488::EGF (Invitrogen; 1:100), and Sytox Blue (Invitrogen, 1:500). For analysis, we size selected the vSVZ cells and excluded for doublets, dead cells and CD45$^+$/Ter119$^+$/O4$^+$ cells as recently described (Kalamakis et al., 2019). Signal acquirement was performed on a BD FACSCanto II at the DKFZ Flow Cytometry Facility and results were analysed using FlowJo v.10.

Cell cycle analysis - CycleFlow

Cell cycle was assessed using CycleFlow as described (Jolly, Fanti, Gräßer, Becker, & Höfer, 2020) with some modifications. CycleFlow was applied to NSCs with or without a pre-treatment of IFN-β. 24 h after cell seeding, either vehicle or IFN-β was added to NSCs for 17 h (this step was skipped in the non-pre-treated NSCs). Then, EdU from the Click-iT Plus EdU Flow Cytometry Assay Kit (ThermoFisher) was added at 10 µM. Cells were incubated 1 h at 37°C 25% CO_2. Cells were collected, washed with DPBS and resuspended in pre-warmed medium containing either vehicle or IFN-β. Cells were then divided in different wells to be incubated and collected at the indicated incubation times (see Figure 1 and S1). At the collection time, cells were collected, dissociated (Accutase®, Sigma) and stained for viability with Zombie Red (Bioleged) following the manufacturer's recommendations. After that, cells were washed and PFA-fixed using the Click-iT Plus EdU Flow Cytometry Assay Kit (ThermoFisher). Fixed cells were kept in 90% methanol DPBS at -20°C until completion of the time-course. Upon all collections, the Click-iT reaction was performed following the manufacturer's recommendations in combination with a final staining with the DNA dye FxCycle Violet reagent (ThermoFisher; 1:1000). Signal acquirement was performed on a BD LSRFortessa Flow Cytometer and results were analysed using FlowJo v.10. Doublets and non-viable cells were excluded from the analysis. Doublets were discriminated using the DNA stain area vs. width. Cell-cycle

progression mathematical inference was performed using uniform priors as already described (Jolly et al., 2020).

Polysome profiling

NSCs were incubated with either vehicle or IFN-β as above explained. Right before cell collection, 100 µg/ml cycloheximide (CHX, EDM Millipore) in H_2O was added to cells and they were incubated 5 min at 37°C 25% CO_2. Cells were collected by centrifugation, washed with ice-cold DPBS containing 100 µg/ml cycloheximide (CHX), and lysed in the Polysome lysis buffer (20 mM Tris-HCl, pH 7.4, 120 mM KCl, 5 mM MgCl2, 14 mM β-mercaptoethanol, 1% NP-40, 100 µg/ml CHX, 1x complete protease inhibitor cocktail (Roche), 100 u/ml RNase Inhibitor (Thermo Fisher)). Lysates of differently treated NSC were loaded at equal amounts for total RNA onto preformed 17.5%-50% gradient of sucrose prepared in 20 mM Tris-HCl pH 7.4, 120 mM KCl, 5 mM MgCl2, 2 mM DTT, 100 µg/ml CHX. Free mRNPs, ribosome subunits, and polysome complexes were resolved by centrifugation for 2.5 h at 35,000 rpm in a SW41 rotor. The content of the tubes was fractionated with the Density Gradient Fractionation System (Teledyne ISCO) allowing for the recording of absorbance at 254 nm. 1 ml fractions were collected for RT-qPCR processing.

RT-qPCR

Total RNA was extracted from cell cultures with the Arcturus PicoPure RNA Isolation Kit (Applied Biosystems). For the fractions of polysome profiling, RNA was purified via phenol/chloroform extraction as described (Faye, Graber, & Holcik, 2014). cDNA was synthesized with the SuperScript VILO cDNA synthesis kit (Thermo Fisher). DNA amplification and detection was performed with the PowerSYBR Green PCR MasterMix (Applied Biosystems) in C1000 Touch Thermal Cycler (Bio-Rad) using QuantiTect (Qiagen) primers (see Table S2: RT-qPCR primers). For the calculation of relative gene expression, the ΔCt method was used. The distribution of analyzed mRNAs across polysome fractions was presented as a percentage of the total amount of the mRNAs for all fractions.

Ribosomal footprinting

Cells were treated with vehicle or IFN-β 48 hours after seeding and incubated at 37°C 25% CO_2 for the corresponding incubation time. Then, NSCs were incubated for 5 min with 0.1 mg/ml CHX at 37°C 25% CO_2. Cells were collected, washed with DPBS supplemented with CHX, and lysed in 150 µl of the Polysome lysis buffer (see Polysome profiling section). Lysates containing 40 µg of total RNA were treated with 100 U of RNaseI (Ambion) for 45 min at room temperature, and the reaction was stopped by addition of 50 U of SUPERaseIn (Ambion). Generated 80S monosomes were collected via centrifugation through 25% sucrose cushion at 100,000 rpm for 1 h in a TLA100.2 rotor, and the pelleted RNA was extracted with the Direct-Zol RNA Miniprep kit (Zimo). Ribosomal RNA was depleted with the Gold Ribo-Zero kit (Illumina). Resulted RNA samples were resolved by electrophoresis in a 15% NOVEX TBE-Urea gel (Thermo Fisher). Gel slices including ribosome footprints corresponding to a fuzzy band of the 26-34 nt size range were cut out from the gel, crushed by centrifugation in 0.5 ml gel-breaker tubes (Segmatic) and extracted in 0.5 ml 10 mM Tris-HCl pH 7.0 by incubation for 15 min at 70°C. RNA was recovered by precipitation with isopropanol in presence of 0.3 M sodium acetate pH 5.5 and 20 µg Glycoblue (Thermo Scientific). Recovered RNA was dephosphorylated with T4 PNK (NEB) in the

absence of ATP. Indexed libraries were generated using the SMARTer smRNA-Seq kit for Illumina (Takara).
For the parallel total mRNA sequencing, we used the same NSC lysates prepared as described above at the amount of 20 µg of total RNA. RNA was extracted with phenol/chloroform as described (Faye et al., 2014). RNA samples were treated with 3 U of TURBO DNase (Ambion) for 15 min at 37°C. RNA was again extracted with phenol/chloroform and recovered with ethanol precipitation in the presence of 0.3 m sodium acetate pH 5.2. Ribosomal RNA was depleted with the Gold Ribo-Zero kit (Illumina). After depletion 80 ng of each RNA sample was used to synthesized cDNA and make a library using the NEBNext Ultra Directional RNA library kit for Illumina (NEB).
Libraries quality was assessed using the Bioanalyzer 2100 (Agilent) and were sequenced in HiSeq 2000 v4.
For the analysis, Reads were trimmed applying the tool TrimGalore version 0.4.4_dev. The adaptor sequence "AGATCGGAAGAGC" (Illumina TruSeq, Sanger iPCR; auto-detected) as well as 3 bp from the 5' end and 15 bp from the 3' end were removed. In addition, sequences that became shorter than 18 bp (after quality trimming) were removed using TrimGalore's default settings. After trimming reads had a length of 33 bp on average. Subsequently, reads were mapped to the mm10 transcriptome build GRC38.93 from ENSEMBL using boWTie version 0.12.7 with its standard options. Reads falling into genes were counted from BAM files applying a suited R/Bioconductor workflow (function SummarizeOverlaps with mode 'Union'). Duplicated reads were removed. For ribosomal footprinting samples, reads in the whole gene body or in the coding part of genes (CDS) were counted separately, for total RNA samples reads in the whole gene body were counted. Next, to get an estimation of the translation efficiency (TE) per gene, log-fold-changes between ribosome protected reads from the CDS and total RNA samples were computed applying DESeq2. The likelihood ratio test (LRT) was applied on the TE analysis upon IFN-β treatment. Genes with positive fold-changes are considered to be enhanced, those with negative ones to be repressed. The gene set enrichment analysis was performed using the clusterProfiler tool from Bioconductor using fold-changes for all expressed genes. Gene ontology terms related to "biological process" with an FDR < 0.05 and highest significance were selected for the plots.

Proteome and phosphoproteome

Cells were treated with vehicle or IFN-β and incubated at 37°C 25% CO_2 for the time specified in the figures. Cell lysates for the proteome and phosphoproteome analysis were prepared as described (Potel, Lin, Heck, & Lemeer, 2018) with some modifications. Briefly, cells were collected, washed and weighted to determine the mass of cells pellets. One volume of the cell pellet was resuspended in six volumes of proteome lysis buffer composed of 100 mM Tris-HCl pH 8.5, 7 M Urea, 1 mM $MgCl_2$, 1 mM sodium ortovanadate, 1% Trition X-100, 1X PhosphoSTOP inhibitor (Roche), 1X Complete EDTA free protease inhibitor (Roche). To improve lysis, cells suspension was sonicated 3 times for 10 s (1 sec on, 1 sec off) with 30 s pause at 40% output using the Fisherbrand Model 120 Sonic Dismembrator (Fisher Scientific). The lysate was clarified by centrifugation at 21000 g, for 1 h at 4°C. Lysates were incubated for 2 h at room temperature. Protein concentration was determined with the Pierce BCA Protein Assay Kit (Thermo Fisher) and 400 µg of total protein for each sample were subjected to metal-affinity enrichment & mass spectrometry at the DKFZ Genomics

and Proteomics Facility. Proteins and phosphopeptides were quantified and analyzed for differential abundance using Perseus45.

Western blot analysis

Cells were collected, washed with DPBS and resuspended in 100 µl of 0.2% SDS, 1 mM vanadate, 1X cOmplete Protease inhibitor cocktail (Roche), 1X PhosphoSTOP inhibitor (Roche) and pass several times through a 23G syringe needle. 15 µg of total protein from cellular lysates were resolved in NuPAGE 10% gels (Thermo Fisher) and transferred to nitrocellulose membranes. The membranes were blocked in 5% BSA in TBS-T buffer and probed overnight with primary antibody. Membranes were washed and reprobed with secondary anti-rabbit or anti-mouse HRP-antibody (Dianova). The signals were developed with the Western Lightning Plus ECL substrate (Perkin Elmer) and scanned using the ChemiDoc Touch Imaging System (Bio-Rad). The Image Lab version 5.2 (Bio-Rad) was used for band intensity quantification.

Luciferase assay

For nucleofection, 3 x 10^6 NSCs were mixed with 5 µg of corresponding DNA with the Amaxa P4 Primary Cell 4D-Nucleofector X Kit S (Lonza) and pulse was delivered using the CA137 programme in a 4D-Nucleofector X Unit (Lonza). Afterwards, the cells were washed, resuspended in medium and separated in three technical replicates. After recovery, cells were treated with IFN-β, Torin1, a combination of both or their corresponding vehicles as stated in the figures. Then, cells were washed and lysed in 1x Passive Lysis buffer from the Dual-Luciferase Reporter Assay System (Promega). Lysis was proceeded on an orbital shaker for 15 min at room temperature. Luciferase Assay reagent was added to each sample, mixed and all volume was transferred into a 96 well White Cliniplate (Thermo Fisher). For *Firefly* luciferase activity the plate was scanned in a Synergy LX mutli-mode reader (BioTek). Then 100 µl of Stop&Glo reagent was added and the plate was scanned again for *Renilla* luciferase. *Renilla* luminescence was normalized to *Firefly* luminescence (with technical triplicates) and the final results were presented as fold change to the control samples.

Plasmid construction

DNA constructs with different WT and mutated 5'UTRs of mouse *Sox2* mRNA were assembled in the psiCheck-2 vector (Promega) including synthetic *Renilla* luciferase gene (hRluc) driven by SV40 early enhancer/promoter and synthetic *Firefly* luciferase gene (hluc+) under HSV-TK promoter. The UTRs flank hRluc open reading frame. The full-length 5'UTRs of mouse *Sox2* (NM_011443.4) and *Rps21* (variant2, NM_025587.2) as well as their mutated variants carrying the deletions of PRM in *Sox2* (5UTRmut *Sox2*; CTCTT deleted), PRM in *Rps21* (5UTRmut *Rps21*; TCCTTTC deleted) were synthesized and inserted into pEX-K4 (*Sox2*) or pEX-A2 (*Rps21*) by Eurofins. The plasmids were used to amplify the UTRs with Phusion High-Fidelity DNA polymerase (NEB) using corresponding primers carrying SfiI and NheI restriction sites to allow the inserts between SV40 promoter and the reading frame of hRluc. The used primers are listed in the Table S1. The final plasmids were designated as 5Sox, 5mutSox, 5Rps21, 5mutRps21.

The full-length 5'UTR of mouse beta actin (*Actb*) mRNA (NM_007393.5) was generated by amplification of cDNA library prepared from NSCs isolated from C57BL/6 mice. For generation of the 5'UTR *Actb*, the used PCR primers were flanked with SfiI

and NheI sites to allow the insertion in front of hRluc reading frame in psiCheck-2 vector (Promega).
The accuracy of cloning was verified by sequencing of the inserts in all generated plasmids from both directions with corresponding primers for sequencing (see Table S3).

Single-cell transcriptomics
To characterize the single-cell transcriptomics of NSCs and their progeny, we made use of TiCY (used as WT) and TiCY-IFNAGRKO mice. In these mice, tamoxifen-induced Cre recombination takes place in neural stem cells in the vSVZ, which express *Tlx* (*Nr2e1*)(H. K. Liu et al., 2008), and will stably activate the production of eYFP labelling NSCs and their progeny.
Tamoxifen (TAM) injection was done in three days as follows: two doses daily of 1mg of tamoxifen in 100 uL of a solution of 10 mg/ml of TAM in EtOH 10% diluted on sunflower seed oil. TiCY young mice were injected with TAM at 10 weeks old and were sacrificed 6 weeks afterwards. TiCY old mice (71 weeks old), TiCY-IFN(A/G)-R young (7 weeks old) and old mice (85 and 98 weeks old) were injected with TAM and were sacrificed 9 weeks afterwards. After animal sacrifice, the vSVZ, striatum, rostral migratory stream and olfactory bulb was isolated. These latter three tissues were pooled together and referred to as Rest of the Brain (RoB). Tissues were processed as described previously (Kremer et al., 2021) and sorted in a BD FACSAria II at the DKFZ Flow Cytometry Facility. For sorting, we size-selected the vSVZ or RoB cells and excluded for doublets, dead cells and $CD45^+/Ter119^+/O4^+$ cells as recently described (Kalamakis et al., 2019). We sorted vSVZ $eYFP^+$ cells and $GLAST^+$ cells. From the RoB, cells that were $eYFP^+$ and $eYFP^-/PSANCAM^{low}$ were sorted. For every condition, 2 mice were used whose cells were labelled with Hashtags oligos (HTO) using the Cell Hashing protocol from Biolegend (TotalSeq-A). All the sorted cells were pooled on the same tube and processed in the Chromium Next GEM Chip G using Chromium Next GEM Single Cell 3' v3.1.
Gene expression libraries were prepared following the manufacturer's protocol (Chromium Next GEM Single Cell 3' v3.1) at the Single-cell open lab at DKFZ and sequenced on a NextSeq2000 V3 PE 100bp at the Sequencing open lab provided by the DKFZ Genomics and Proteomics Core Facility. Each condition (TiCY and TiCY-IFNAGRKO young and old) was processed on a separate 10X reaction. Hashtags libraries were processed according to the manufacturer's instruction (Biolegend) and were sequenced on a NextSeq 500 Mid output PE 75bp at the DKFZ Genomics and Proteomics Core Facility.

Single-cell transcriptomic data analysis
To derive a "NSC type I Interferon Response" signature we used the 16h IFN-β treated Ribo-Seq transcriptomic libraries. Reads were trimmed using trimgalore 0.6.6 using default settings and mapped and quantified using STAR 2.7.7a with --quantMode GeneCounts. Star outputs were concatenated and read into R 4.0.5 where DESeq2 1.30.1 was used to compute differential expression between treated and untreated samples. The genes with the 300 most significantly changed genes after multiple-testing correction from a one-sided Wald test (increased expression) were chosen as our "NSC Type I Interferon Response" gene set.
For the single-cell libraries analysis, we filtered them using the 10x index-hopping-filter 1.0.1 and thereafter quantified using kallisto|bustools's lamanno workflow (kb_python 0.26.3). Hashtag libraries were quantified using CITE-seq-Count 1.4.5. Count matrices

were read into scanpy 1.6.0 and preprocessed by filtering out genes present in less than three cells and cells with less than 100 genes. Doublets were called and removed with scrublet 0.2.1. Cells with less than 10% mitochondrial UMIs, 70-6000 genes and 1000-20000 UMIs were retained as quality cells. Counts were normalised (to a target sum of 10000) and log1p transformed using scanpy methods. A UMAP was computed from 50PCs computed on scaled counts. Main clusters were identified in UMAP using DBSCAN (scikit-learn 0.22.2.post1). An auxilliary leiden clustering was computed. The largest DBSCAN cluster was identified as the lineage cluster based on marker expression. Non-subventricular astrocytes were identified and removed from this cluster by inspecting the fraction of SVZ hashtags in each cell. Other clusters were named by summed expression of celltype specific-markers (Pecam1, Prom1 and Cldn5 for endothelials, Itgam and Ptprc for microglia, Rbfox3, Calb2, Nefl and Th for neurons). Diffusion pseudotime (from scanpy) was run on the lineage cluster using the cell with the highest Aqp4 expression as the root cell. Pseudotime was then binned into qNSC1, qNSC2, aNSC, TAP and NB based on visual inspection of the expression of well-known markers Aqp4, Egfr, Dcx, Mki67, S100b. Hashtag samples were called for each cell as the maximum posterior from a multinomial mixture model (R 4.0.5 package mixtools 1.2.0) with 5 components (one for each hashtag and an extra component for no hashtags).
Gene set scores were then computed for each cell by summing up the normalised (per cell to 1000000 UMIs) and log1p-transformed expression of genes from a given set. Group-wise gene set scores were then computed as the avearge of all of the cell's scores in a given group of interest. Scores were computed for each replicate, celltype, age and genotype combination for MSigDB's "HALLMARK_INFLAMMATORY_RESPONSE", "HALLMARK_INTERFERON_ALPHA_RESPONSE" genesets, as well as the gene set identified by Wu et al. 2018(Wu et al., 2018) and our "NSC Type I Interferon Response".

IFNAGR KO Modelling

We built on the previously established mathematical model of cell population dynamics (Kalamakis et al., 2019), describing counts of quiescent (non-cycling) and active (cycling) stem cells. The model is given by a system of ordinary differential equations:

$$\frac{d}{dt}\text{qNSC} = -r \cdot \text{qNSC} + 2 \cdot b \cdot p_s \cdot \text{aNSC},$$

$$\frac{d}{dt}\text{aNSC} = r \cdot \text{qNSC} - p_s \cdot \text{aNSC}.$$

The parameter r describes the activation rate that may exponentially decrease in time

$$r(t) = r_0 \cdot e^{-\beta_r \cdot t}.$$

Self-renewal is modeled by a function b

$$b(t) = \frac{1}{2}\left(1 + e^{-\beta_b \cdot t} \cdot (2 \cdot b_0 - 1)\right).$$

The choice of this function follows the assumptions that self-renewal probability is not larger than ½ and may be a constant or increasing in time function.
The remaining parameter $p_s = \log(2)/(17.5/24) \approx 0.9506$ corresponds to the cell cycle rate. It was chosen from literature, following our previous publication (Kalamakis et al., 2019). In summary, the model is characterised by free parameters r_0, b_0, β_b and β_r. The initial value additionally provides the parameter NSC_0 which was used to compute initial values for the specific compartments from the steady state ratio (Supplementary Data 1).

Parameters were estimated using a multi-start box-constrained weighted-least-squares approach. The objective functions were built using new FACS quantifications for the total numbers of stem cells and the fraction of actively cycling neural stem cells from our previous publication. We applied solvers provided and chosen by the DifferentialEquations.jl package. Weights were computed as the inverse standard deviation for each age and genotype combination. Starting values were sampled from within reasonable bounds using Latin Hypercubes computed by the LatinHypercubeSampling.jl library, each was then optimized using a box constrained optimizer from the Optim.jl library. The best parameter estimates were kept as the optimum. To aid in model selection, AIC_c was computed for each model and dataset combination.
Finally, we estimated parameters for models with population-dependent self-renewal probabilities, described by a Hill function:

$$b(\mathrm{NSC}) = 1 - \frac{1}{1 + \left(\frac{k_b}{\mathrm{NSC}}\right)^{n_b}}.$$

We estimated these with a single k_b for both genotypes. The parameter n_b was estimated individually per-genotype (IFN-dependent self-renewal) or shared (IFN-independent self-renewal) to provide the two scenarios of self-renewal dependence on interferons.

IFNAGR KO simulations at arbitrary time points

To simulate the age-specific dynamics of the IFNAGR KO, we built a model with a time-dependent switch in the parameter functions. At the intervention age, the parameter functions are switched from the previously estimated WT parameter functions to their IFNAGR KO counterparts. We simulated this intervention model for varying intervention ages. For each simulation we computed the number of stem cell loss at 660 days age compared to the wildtype. We also computed the progenitor production as the cell flux from active neural stem cells to progenitors. We then integrated progenitor production from 0 to 700 as the total life-long progenitors produced.

QUANTIFICATION AND STATISTICAL ANALYSIS

Biological replicates “n” in the figures refer to biological replicates as of either different mice or different NSCs cultures extracted from different mice. Plotted bars represent mean and plotted error bars represent standard deviation from different biological replicates. Only biological replicates were considered for statistical analyses. Statistical tests were performed as indicated in each figure legend with a significance level of α = 0,05.

Supplemental Figures

Figure S1

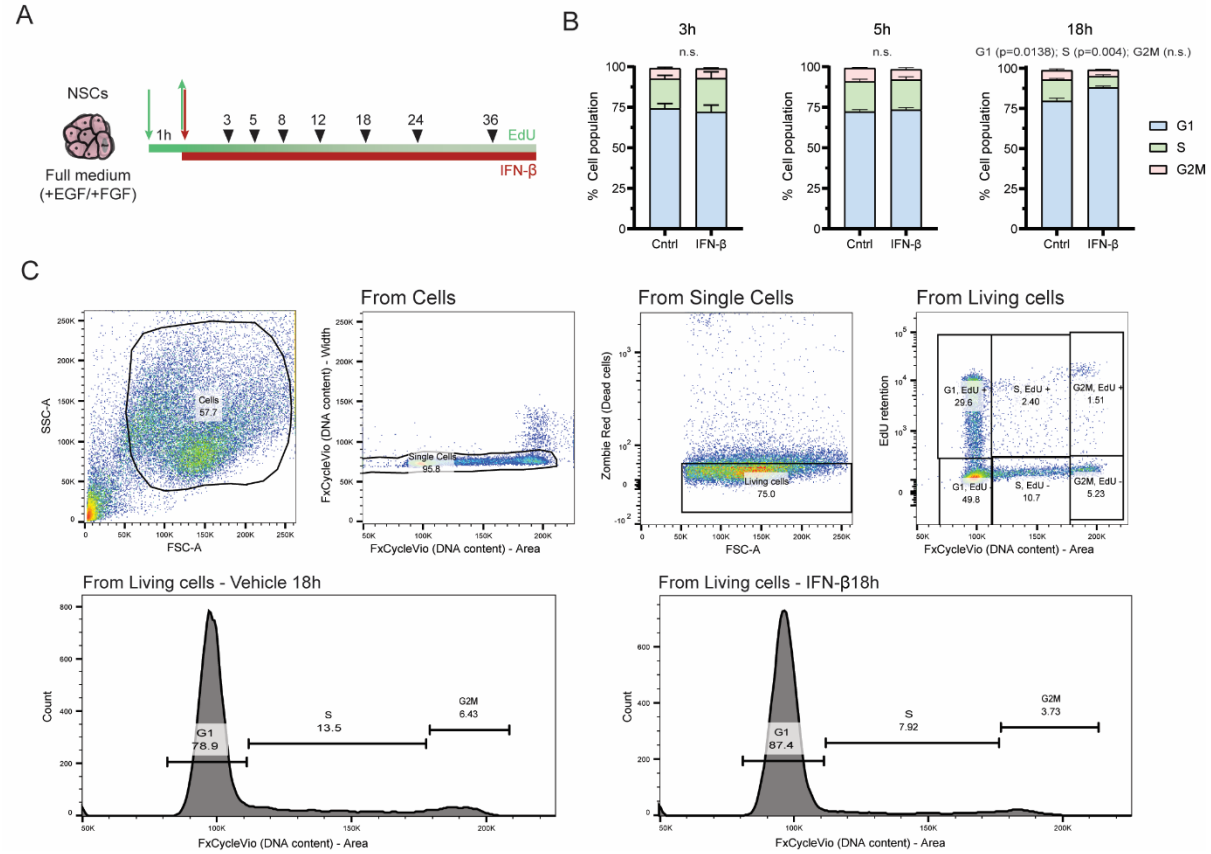

Figure S1. IFN-β induce cell cycle exit in NSCs, Related to Figure 1

A) EdU and IFN-β exposure experimental scheme. **B)** Distributions of NSCs in G_1, S and G2M based on their DNA content at different time points are depicted. Data is normalized is represented as mean ± SD. Two-way ANOVA with Ŝídák's multiple comparisons test. n = 3. p ≡ p-value. **C)** Gating strategy for quantification of cell cycle states for Cycleflow or general cell cycle stages G_1, S and G_2M (lower panels).

Figure S2

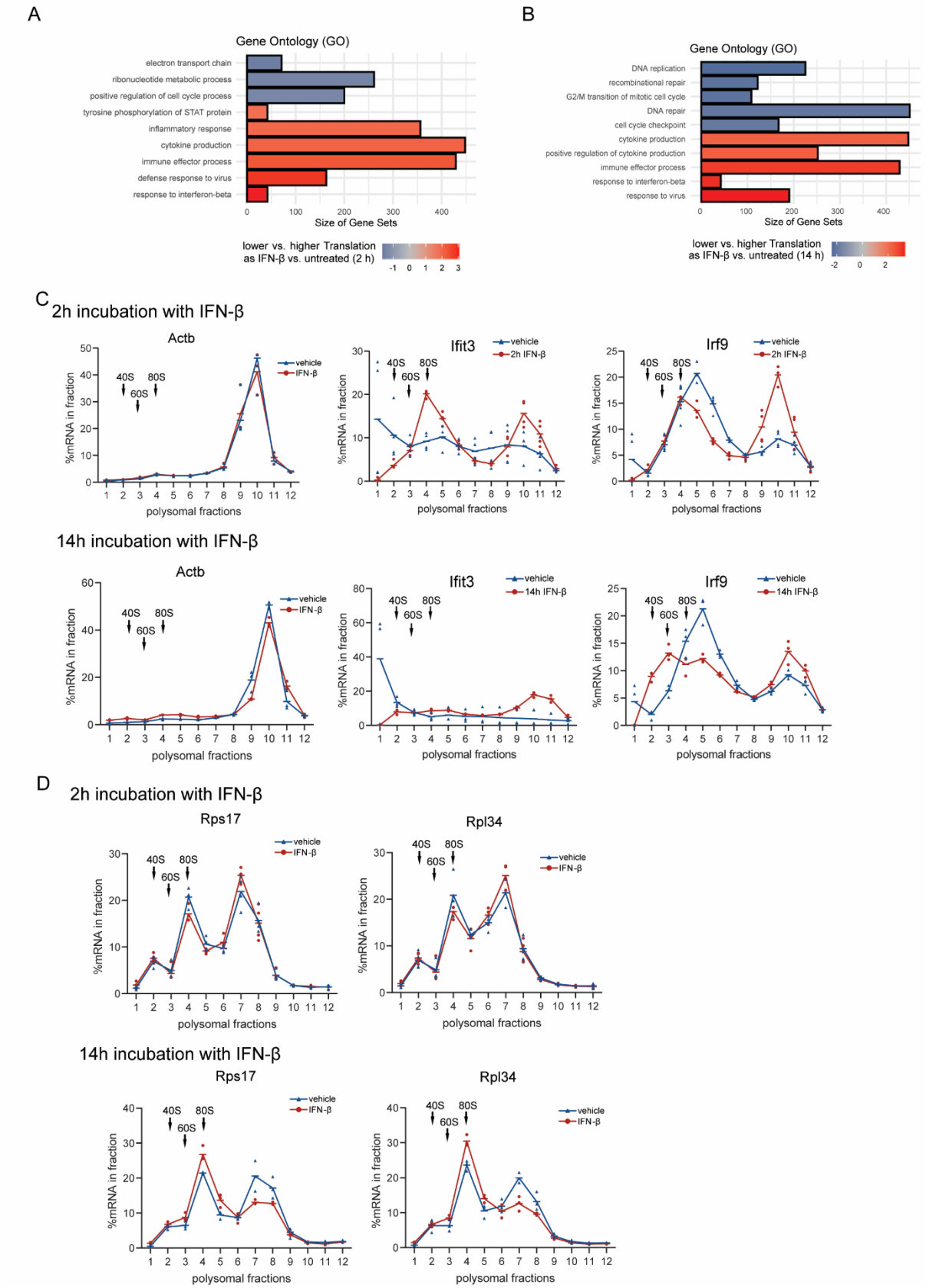

Figure S2. IFN-β induce a biphasic control of mRNA translation in NSCs, Related to Figure 2
A) & B) Results of Ribo-Seq depicting translation efficiency as the interaction of log2 fold changes (LFC) between footprints (ribosome protected reads) and total RNA at 2h and 14h IFN-β treatment. FDR < 10%, LR-Test. Genes with a p-value <0.1 after FDR correction are highlighted. The associated

GO terms are depicted. n = 3. **C)** Polysome profiling (RT-qPCR) of actin beta and of the interferon stimulated genes (ISGs) Ifit3 and Irf9 upon 2h and 14h IFN-β treatment. Hyphens represent mean of biological replicates. Arrows indicate the 40S, 60S and 80S subunits of the ribosome. n = 3-4. **D)** Polysome profiling (RT-qPCR) of *Rps17* and *Rpl34* upon 2h and 14h IFN-β treatment. Hyphens represent mean of biological replicates. Arrows indicate the 40S, 60S and 80S subunits of the ribosome. n = 3-4.

Figure S3

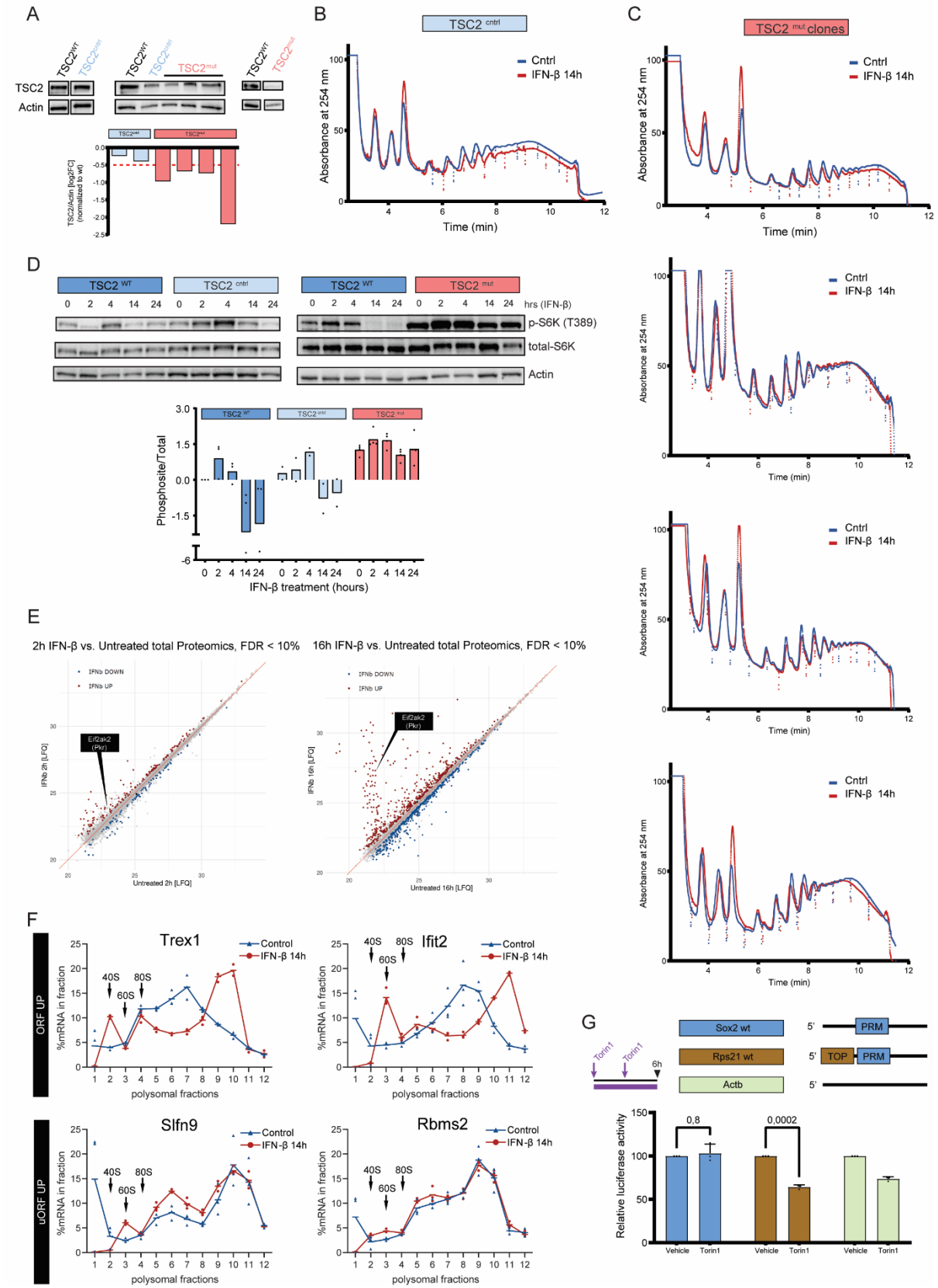

Figure S3. The biphasic control of mTORC1 by IFN-β relies on TSC2, PKR and eIF2α. Related to Figure 3

A) WB images and quantifications of TSC2 relative to actin beta and normalized to TSC2^{WT} NSCs in different CRISPR-mutated (TSC2^{mut}) or CRSPR-non-mutated (TSC2^{cntrl}) NSC clones.

(B & C) Polysome profiles of CRISPR-mediated $TSC2^{cntrl}$ and $TSC2^{mut}$ NSC clones treated with IFN-β (red) as compared to control (blue). Each plot represents different $TSC2^{mut}$ NSC clones. **D)** Representative WB images and quantifications (log2FC) of p-p70S6K^{Thr389} in $TSC2^{WT}$, $TSC2^{cntrl}$ & $TSC2^{mut}$ NSCs treated with IFN-β and normalized to vehicle (t=0h) $TSC2^{WT}$. Bars represent the mean value. n = 2-4 clonal replicates. **E)** Relate label-free quantification (LFQ) of proteomics from WT NSCs untreated or treated with IFN-β for 2h or 16h. **F)** Polysome profiling (RT-qPCR) of genes displaying upregulation of footprints in the ORF (Trex1 and Ifit2) compared to genes with an upregulation in uORFs (Slfn9 and Rbms2) upon 14h IFN-β treatment. Hyphens represent mean of biological replicates. Arrows indicate the 40S, 60S and 80S subunits of the ribosome. n = 3. **G)** Experimental layout (left) & 5'UTR constructs priming *renilla* luciferase. TOP = 5'Terminal Oligopyrimidine motif; PRM = 5' Pyrimidine Rich Motif. Luciferase activity (right) controlled by the upstream 5'UTR fragment from Sox2, Rps21 and Actb. Data is normalized to vehicle and is represented as mean ± SD. n = 3 biological replicates. Two-way ANOVA test with Ŝídák's multiple comparison test (p-value specified).

Figure S4

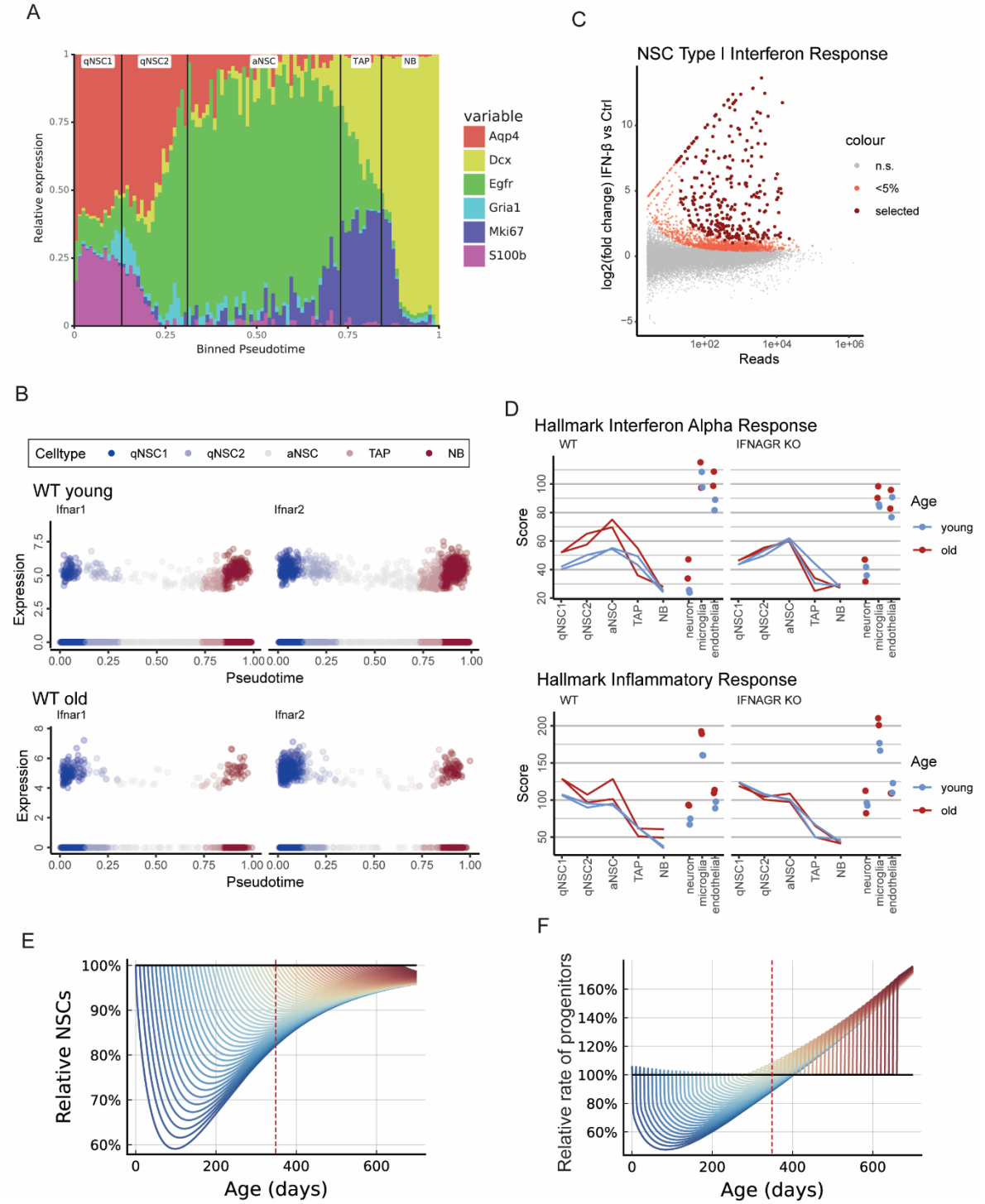

Figure S4. Inference of intrinsic IFN signature and modeling of interferon receptors removal along lifespan. Related to Figure 4

A) Relative gene expression of relevant markers for cell types along pseudotime. Black lines denote cuts between cell types. **B)** Relative expression of type I IFN receptors in young and old wildtype cells over pseudotime colored by lineage cell types. **C)** MA plot showing differential expression between IFN-β 16h treated bulk cells and Control cells. Light red dots are significantly upregulated (one-sided Wald test), dark red dots are the top 300 genes selected as the "NSC Type I Interferon Response". **D)** Scores derived for the different gene signatures (Hallmark Inflammatory Response and Hallmark Interferon Alpha Response from MSigDB) and cell types in our analysis at varying ages in wildtype (WT) and IFNAGR KO cells. n = 2 biological replicates per age and genotype. **E)** Induced interferon knockout simulations (colored, each color represents a different intervention timepoint) of relative loss of stem cells across age compared to wildtype simulations (black; 100%). Dashed red line denotes age 350

days. **F)** The relative rate at which progenitors are produced $(2\ p_s\ (1-b)\ aNSC)$ from NSCs for induced interferon knockout simulations with interferon dependent self-renewal (colored, each color represents a different intervention timepoint) compared to WT simulations (black; 100%). Dashed red line denotes age 350 days.

Table S1: List of relevant phosphosites. Related to Figure 3, S3.

Protein	Phosphosite	log2FC (2h)	log2FC (16h)
Akt1	S473	0.1	-1
Irs1	Y608	1.2	0.3
Irs1	S1134	0.9	-2.3
Irs1	S1137	0.2	-1.7
Eif2ak2	S32	0.1	4.2
Eif2ak2	S110	0.4	3.3
Eif2ak2	S163	-0.2	2.4
Eif2ak2	S223	0.5	2.1
Eif2ak2	S240	-1	3.1
Ccnd1	T286	1.9	0.3

Table S1. Phosphosites – Related to Figure 3, S3

References

Alspach, E., Lussier, D. M., & Schreiber, R. D. (2019). Interferon γ and its important roles in promoting and inhibiting spontaneous and therapeutic cancer immunity. *Cold Spring Harbor Perspectives in Biology*, *11*(3), 1–22. https://doi.org/10.1101/cshperspect.a028480

Artegiani, B., Lindemann, D., & Calegari, F. (2011). Overexpression of cdk4 and cyclinD1 triggers greater expansion of neural stem cells in the adult mouse brain. *Journal of Experimental Medicine*, *208*(5), 937–948. https://doi.org/10.1084/jem.20102167

Avni, D., Biberman, Y., & Meyuhas, O. (1996). The 5′ Terminal Oligopyrimidine Tract Confers Translational Control on Top Mrnas in a Cell Type-and Sequence Context-Dependent Manner. *Nucleic Acids Research*, *25*(5), 995–1001. https://doi.org/10.1093/nar/25.5.995

Baruch, K., Deczkowska, A., David, E., Castellano, J. M., Miller, O., Kertser, A., … Schwartz, M. (2014). Aging-induced type I interferon response at the choroid plexus negatively affects brain function. *Science*, *346*(6205), 89 LP – 93. https://doi.org/10.1126/science.1252945

Baser, A., Skabkin, M., Kleber, S., Dang, Y., Gülcüler Balta, G. S., Kalamakis, G., … Martin-Villalba, A. (2019). Onset of differentiation is post-transcriptionally controlled in adult neural stem cells. *Nature*, *566*(7742), 100–104. https://doi.org/10.1038/s41586-019-0888-x

Baser, A., Skabkin, M., & Martin-Villalba, A. (2017). Neural Stem Cell Activation and the Role of Protein Synthesis. *Brain Plasticity*, *3*, 1–15. https://doi.org/10.3233/BPL-160038

Blanco, S., Bandiera, R., Popis, M., Hussain, S., Lombard, P., Aleksic, J., … Frye, M. (2016). Stem cell function and stress response are controlled by protein synthesis. *Nature*, *534*(7607), 335–340. https://doi.org/10.1038/nature18282

Blank, T., Detje, C. N., Spieß, A., Hagemeyer, N., Brendecke, S. M., Wolfart, J., … Prinz, M. (2016). Brain Endothelial- and Epithelial-Specific Interferon Receptor Chain 1 Drives Virus-Induced Sickness Behavior and Cognitive Impairment. *Immunity*, *44*(4), 901–912. https://doi.org/10.1016/j.immuni.2016.04.005

Blank, T., & Prinz, M. (2017). Type I interferon pathway in CNS homeostasis and neurological disorders. *Glia*, *65*(9), 1397–1406. https://doi.org/10.1002/glia.23154

Carrasco-Garcia, E., Moreno-Cugnon, L., Garcia, I., Borras, C., Revuelta, M., Izeta, A., … Matheu, A. (2019). SOX2 expression diminishes with ageing in several tissues in mice and humans. *Mechanisms of Ageing and Development*, *177*, 30–36. https://doi.org/10.1016/j.mad.2018.03.008

Copps, K. D., & White, M. F. (2012). Regulation of insulin sensitivity by serine/threonine phosphorylation of insulin receptor substrate proteins IRS1 and IRS2. *Diabetologia*, *55*(10), 2565–2582. https://doi.org/10.1007/s00125-012-2644-8

Daynac, M., Morizur, L., Chicheportiche, A., Mouthon, M. A., & Boussin, F. D. (2016). Age-related neurogenesis decline in the subventricular zone is associated with specific cell cycle regulation changes in activated neural stem cells. *Scientific Reports*, *6*(February), 1–10. https://doi.org/10.1038/srep21505

Demerdash, Y., Kain, B., Essers, M. A. G., & King, K. Y. (2021). Yin and Yang: The dual effects of interferons on hematopoiesis. *Experimental Hematology*, *96*, 1–12. https://doi.org/10.1016/j.exphem.2021.02.002

Dulken, B. W., Buckley, M. T., Navarro Negredo, P., Saligrama, N., Cayrol, R., Leeman, D. S., … Brunet, A. (2019). Single-cell analysis reveals T cell infiltration in old neurogenic niches. *Nature*. https://doi.org/10.1038/s41586-019-1362-5

Esposito, D. L., Li, Y., Cama, A., & Quon, M. J. (2001). Tyr612 and Tyr632 in human insulin receptor substrate-1 are important for full activation of insulin-stimulated phosphatidylinositol 3-kinase activity and translocation of GLUT4 in adipose cells. *Endocrinology*, *142*(7), 2833–2840. https://doi.org/10.1210/endo.142.7.8283

Faye, M. D., Graber, T. E., & Holcik, M. (2014). Assessment of selective mRNA translation in mammalian cells by polysome profiling. *Journal of Visualized Experiments*, (92), 1–8. https://doi.org/10.3791/52295

Fernández-Fernández, L., Comes, G., Bolea, I., Valente, T., Ruiz, J., Murtra, P., … Unzeta, M. (2012). LMN diet, rich in polyphenols and polyunsaturated fatty acids, improves mouse cognitive decline associated with aging and Alzheimer's disease. *Behavioural Brain Research*, *228*(2), 261–271. https://doi.org/10.1016/J.BBR.2011.11.014

Friend, K., Brooks, H. A., Propson, N. E., Thomson, J. A., & Kimble, J. (2015). Embryonic stem cell growth factors regulate eIF2α phosphorylation. *PLoS ONE*, *10*(9), 1–15. https://doi.org/10.1371/journal.pone.0139076
Fulop, T., Larbi, A., Dupuis, G., Page, A. Le, Frost, E. H., Cohen, A. A., … Franceschi, C. (2018). Immunosenescence and inflamm-aging as two sides of the same coin: Friends or Foes? *Frontiers in Immunology*, *8*(JAN). https://doi.org/10.3389/fimmu.2017.01960
Gal-Ben-Ari, S., Barrera, I., Ehrlich, M., & Rosenblum, K. (2019). PKR: A kinase to remember. *Frontiers in Molecular Neuroscience*, *11*(January), 1–20. https://doi.org/10.3389/fnmol.2018.00480
Glück, S., & Ablasser, A. (2019). Innate immunosensing of DNA in cellular senescence. *Current Opinion in Immunology*, *56*, 31–36. https://doi.org/10.1016/j.coi.2018.09.013
Guo, Y., Yang, K., Harwalkar, J., Nye, J. M., Mason, D. R., Garrett, M. D., … Stacey, D. W. (2005). Phosphorylation of cyclin D1 at Thr 286 during S phase leads to its proteasomal degradation and allows efficient DNA synthesis. *Oncogene*, *24*(16), 2599–2612. https://doi.org/10.1038/sj.onc.1208326
Haas, S., Hirche, C., Schnell, A., Sönmezer, C., Langstein, J., Wurzer, S., … Essers, M. A. G. (2017). A Stem Cell-Based Epigenetic Memory Mediates Interferon Response-Heterogeneity within the Hematopoietic System. *Blood*, *130*(Suppl_1), 634–634. https://doi.org/10.1182/blood.v130.suppl_1.634.634
Hou, Q., Huang, J., Ayansola, H., Masatoshi, H., & Zhang, B. (2021). Intestinal Stem Cells and Immune Cell Relationships: Potential Therapeutic Targets for Inflammatory Bowel Diseases. *Frontiers in Immunology*, *11*(January), 1–14. https://doi.org/10.3389/fimmu.2020.623691
Hsu, P. P., Kang, S. A., Rameseder, J., Zhang, Y., Ottina, K. A., Lim, D., … Sabatini, D. M. (2011). The mTOR-regulated phosphoproteome reveals a mechanism of mTORC1-mediated inhibition of growth factor signaling. *Science*, *332*(6035), 1317–1322. https://doi.org/10.1126/science.1199498
Huang, S., Hendriks, W., Althage, A., Hemmi, S., Bluethmann, H., Kamijo, R., … Aguet, M. (1993). Immune response in mice that lack the interferon-γ receptor. *Science*, *259*(5102), 1742–1745. https://doi.org/10.1126/science.8456301
Ivashkiv, L. B., & Donlin, L. T. (2014). Regulation of type i interferon responses. *Nature Reviews Immunology*, *14*(1), 36–49. https://doi.org/10.1038/nri3581
Jin, W. N., Shi, K., He, W., Sun, J. H., Van Kaer, L., Shi, F. D., & Liu, Q. (2021). Neuroblast senescence in the aged brain augments natural killer cell cytotoxicity leading to impaired neurogenesis and cognition. *Nature Neuroscience*, *24*(1), 61–73. https://doi.org/10.1038/s41593-020-00745-w
Jolly, A., Fanti, A.-K., Gräßer, I., Becker, N. B., & Höfer, T. (2020). CycleFlow quantifies cell-cycle heterogeneity in vivo. *BioRxiv*, 2020.09.10.291088.
Kalamakis, G., Brüne, D., Ravichandran, S., Bolz, J., Ziebell, F., Stiehl, T., … Martin-Villalba, A. (2019). Quiescence Modulates Stem Cell Maintenance and Regenerative Capacity in the Aging Brain Article Quiescence Modulates Stem Cell Maintenance and Regenerative Capacity in the Aging Brain. https://doi.org/10.1016/j.cell.2019.01.040
Karlsson, H. K. R., Kasahara, A., Ikeda, M., Chibalin, A. V., Harada, J., Rydén, M., … Zierath, J. R. (2021). Quantitative phosphoproteomic analysis of IRS1 in skeletal muscle from men with normal glucose tolerance or type 2 diabetes: A case-control study. *Metabolism: Clinical and Experimental*, *118*, 154726. https://doi.org/10.1016/j.metabol.2021.154726
Kim, J., & Guan, K. L. (2019). mTOR as a central hub of nutrient signalling and cell growth. *Nature Cell Biology*, *21*(1), 63–71. https://doi.org/10.1038/s41556-018-0205-1
Kremer, L. P. M., Cerrizuela, S., Dehler, S., Stiehl, T., Weinmann, J., Abendroth, H., … Martin-Villalba, A. (2021). High throughput screening of novel AAV capsids identifies variants for transduction of adult NSCs within the subventricular zone. *Molecular Therapy - Methods & Clinical Development*, *23*(December), 33–50. https://doi.org/10.1016/j.omtm.2021.07.001
Kroczynska, B., Mehrotra, S., Arslan, A. D., Kaur, S., & Platanias, L. C. (2014). Regulation of interferon-dependent mRNA translation of target genes. *Journal of Interferon and Cytokine Research*, *34*(4), 289–296. https://doi.org/10.1089/jir.2013.0148
Lange, C., Huttner, W. B., & Calegari, F. (2009). Cdk4/CyclinD1 Overexpression in Neural Stem Cells Shortens G1, Delays Neurogenesis, and Promotes the Generation and Expansion of Basal Progenitors. *Cell Stem Cell*, *5*(3), 320–331. https://doi.org/10.1016/j.stem.2009.05.026
Langlais, P., Yi, Z., Finlayson, J., Luo, M., Mapes, R., De Filippis, E., … Mandarino, L. J. (2011). Global IRS-1 phosphorylation analysis in insulin resistance. *Diabetologia*, *54*(11), 2878–2889. https://doi.org/10.1007/s00125-011-2271-9
Lekmine, F., Sassano, A., Uddin, S., Smith, J., Majchrzak, B., Brachmann, S. M., … Platanias, L. C. (2004). Interferon-γ engages the p70 S6 kinase to regulate phosphorylation of the 40S S6 ribosomal protein. *Experimental Cell Research*, *295*(1), 173–182. https://doi.org/10.1016/j.yexcr.2003.12.021
Lekmine, F., Uddin, S., Sassano, A., Parmar, S., Brachmann, S. M., Majchrzak, B., … Platanias, L. C. (2003). Activation of the p70 S6 kinase and phosphorylation of the 4E-BP1 repressor of mRNA translation by type I interferons. *Journal of Biological Chemistry*, *278*(30), 27772–27780. https://doi.org/10.1074/jbc.M301364200
Liu, G. Y., & Sabatini, D. M. (2020). mTOR at the nexus of nutrition, growth, ageing and disease. *Nature Reviews Molecular Cell Biology*, *21*(4), 183–203. https://doi.org/10.1038/s41580-019-0199-y
Liu, H. K., Belz, T., Bock, D., Takacs, A., Wu, H., Lichter, P., … Schütz, G. (2008). The nuclear receptor tailless is required for neurogenesis in the adult subventricular zone. *Genes and Development*, *22*(18), 2473–2478. https://doi.org/10.1101/gad.479308
Llorens-Bobadilla, E., Zhao, S., Baser, A., Saiz-Castro, G., Zwadlo, K., & Martin-Villalba, A. (2015). Single-Cell Transcriptomics Reveals a Population of Dormant Neural Stem Cells that Become Activated upon Brain Injury. *Cell Stem Cell*, *17*(3), 329–340. https://doi.org/10.1016/j.stem.2015.07.002
Ma, X. M., & Blenis, J. (2009). Molecular mechanisms of mTOR-mediated translational control. *Nature Reviews Molecular Cell Biology*, *10*(5), 307–318. https://doi.org/10.1038/nrm2672
Marqués-Torrejón, M. Á., Porlan, E., Banito, A., Gómez-Ibarlucea, E., Lopez-Contreras, A. J., Fernández-Capetillo, Ó., … Fariñas, I. (2013). Cyclin-dependent kinase inhibitor p21 controls adult neural stem cell expansion by regulating Sox2 gene expression. *Cell Stem Cell*, *12*(1), 88–100. https://doi.org/10.1016/j.stem.2012.12.001
Mazewski, C., Perez, R. E., Fish, E. N., & Platanias, L. C. (2020). Type I Interferon (IFN)-Regulated Activation of Canonical and Non-Canonical Signaling Pathways. *Frontiers in Immunology*, *11*(November), 1–13. https://doi.org/10.3389/fimmu.2020.606456
Mirzadeh, Z., Doetsch, F., Sawamoto, K., Wichterle, H., & Alvarez-Buylla, A. (2010). The subventricular zone en-face: Wholemount staining and ependymal flow. *Journal of Visualized Experiments*, (39), 1–8. https://doi.org/10.3791/1938
Molofsky, A. V., Slutsky, S. G., Joseph, N. M., He, S., Pardal, R., Krishnamurthy, J., … Morrison, S. J. (2006). Increasing

p16INK4a expression decreases forebrain progenitors and neurogenesis during ageing. *Nature*, *443*(7110), 448–452. https://doi.org/10.1038/nature05091
Muendlein, H. I., Sarhan, J., Liu, B. C., Connolly, W. M., Schworer, S. A., Smirnova, I., … Poltorak, A. (2020). Constitutive Interferon Attenuates RIPK1/3-Mediated Cytokine Translation. *Cell Reports*, *30*(3), 699-713.e4. https://doi.org/10.1016/j.celrep.2019.12.073
Müller, U., Steinhoff, U., Reis, L. F. L., Hemmi, S., Pavlovic, J., Zinkernagel, R. M., & Aguet, M. (1994). Functional role of type I and type II interferons in antiviral defense. *Science*, *264*(5167), 1918–1921. https://doi.org/10.1126/science.8009221
Nakamura, T., Furuhashi, M., Li, P., Cao, H., Tuncman, G., Sonenberg, N., … Hotamisligil, G. S. (2010). Double-Stranded RNA-Dependent Protein Kinase Links Pathogen Sensing with Stress and Metabolic Homeostasis. *Cell*, *140*(3), 338–348. https://doi.org/10.1016/j.cell.2010.01.001
Ogrodnik, M., Zhu, Y., Langhi, L. G. P., Tchkonia, T., Krüger, P., Fielder, E., … Jurk, D. (2019). Obesity-Induced Cellular Senescence Drives Anxiety and Impairs Neurogenesis. *Cell Metabolism*, *29*(5), 1061-1077.e8. https://doi.org/10.1016/j.cmet.2018.12.008
Payea, M. J., Anerillas, C., Tharakan, R., & Gorospe, M. (2021). Translational Control during Cellular Senescence. *Molecular and Cellular Biology*, *41*(2), 1–14. https://doi.org/10.1128/mcb.00512-20
Piazzi, M., Bavelloni, A., Faenza, I., & Blalock, W. (2020). Glycogen synthase kinase (GSK)-3 and the double-strand RNA-dependent kinase, PKR: When two kinases for the common good turn bad. *Biochimica et Biophysica Acta - Molecular Cell Research*, *1867*(10), 118769. https://doi.org/10.1016/j.bbamcr.2020.118769
Pietras, E. M., Lakshminarasimhan, R., Techner, J. M., Fong, S., Flach, J., Binnewies, M., & Passegué, E. (2014). Re-entry into quiescence protects hematopoietic stem cells from the killing effect of chronic exposure to type I interferons. *Journal of Experimental Medicine*, *211*(2), 245–262. https://doi.org/10.1084/jem.20131043
Platanias, L. C. (2005). Mechanisms of type-I- and type-II-interferon-mediated signalling. *Nature Reviews Immunology*, *5*(5), 375–386. https://doi.org/10.1038/nri1604
Potel, C. M., Lin, M. H., Heck, A. J. R., & Lemeer, S. (2018). Defeating major contaminants in Fe3- immobilized metal ion affinity chromatography (IMAC) phosphopeptide enrichment. *Molecular and Cellular Proteomics*, *17*(5), 1028–1034. https://doi.org/10.1074/mcp.TIR117.000518
Ran, F. A., Hsu, P. D., Wright, J., Agarwala, V., Scott, D. A., & Zhang, F. (2013). Genome engineering using the CRISPR-Cas9 system. *Nature Protocols*, *8*(11), 2281–2308. https://doi.org/10.1038/nprot.2013.143
Romero-Pozuelo, J., Figlia, G., Kaya, O., Martin-Villalba, A., & Teleman, A. A. (2020). Cdk4 and Cdk6 Couple the Cell-Cycle Machinery to Cell Growth via mTORC1. *Cell Reports*, *31*(2). https://doi.org/10.1016/j.celrep.2020.03.068
Rozengurt, E., Soares, H. P., & Sinnet-Smith, J. (2014). Suppression of feedback loops mediated by pi3k/mtor induces multiple overactivation of compensatory pathways: An unintended consequence leading to drug resistance. *Molecular Cancer Therapeutics*, *13*(11), 2477–2488. https://doi.org/10.1158/1535-7163.MCT-14-0330
Sarbassov, D. D., Guertin, D. A., Ali, S. M., & Sabatini, D. M. (2005). Phosphorylation and Regulation of Akt/PKB by the Rictor-mTOR Complex. *Science*, *307*(5712), 1098 LP – 1101. https://doi.org/10.1126/science.1106148
Stanifer, M. L., Guo, C., Doldan, P., & Boulant, S. (2020). Importance of Type I and III Interferons at Respiratory and Intestinal Barrier Surfaces. *Frontiers in Immunology*, *11*(December), 1–14. https://doi.org/10.3389/fimmu.2020.608645
Stemmer, M., Thumberger, T., Del Sol Keyer, M., Wittbrodt, J., & Mateo, J. L. (2015). CCTop: An intuitive, flexible and reliable CRISPR/Cas9 target prediction tool. *PLoS ONE*, *10*(4), 1–11. https://doi.org/10.1371/journal.pone.0124633
Su, Q., Wang, S., Baltzis, D., Qu, L. K., Raven, J. F., Li, S., … Koromilas, A. E. (2007). Interferons induce tyrosine phosphorylation of the eIF2α kinase PKR through activation of Jak1 and Tyk2. *EMBO Reports*, *8*(3), 265–270. https://doi.org/10.1038/sj.embor.7400891
Su, X., Yu, Y., Zhong, Y., Giannopoulou, E. G., Hu, X., Liu, H., … Ivashkiv, L. B. (2015). Interferon-γ regulates cellular metabolism and mRNA translation to potentiate macrophage activation. *Nature Immunology*, *16*(8), 838–849. https://doi.org/10.1038/ni.3205
Syedbasha, M., Bonfiglio, F., Linnik, J., Stuehler, C., Wüthrich, D., & Egli, A. (2020). Interferon-λ Enhances the Differentiation of Naive B Cells into Plasmablasts via the mTORC1 Pathway. *Cell Reports*, *33*(1). https://doi.org/10.1016/j.celrep.2020.108211
Tahmasebi, S., Amiri, M., & Sonenberg, N. (2019). Translational control in stem cells. *Frontiers in Genetics*, *10*(JAN), 1–9. https://doi.org/10.3389/fgene.2018.00709
Thoreen, C. C., Chantranupong, L., Keys, H. R., Wang, T., Gray, N. S., & Sabatini, D. M. (2012). A unifying model for mTORC1-mediated regulation of mRNA translation. *Nature*, *485*(7396), 109–113. https://doi.org/10.1038/nature11083
Topacio, B. R., Zatulovskiy, E., Cristea, S., Xie, S., Tambo, C. S., Rubin, S. M., … Skotheim, J. M. (2019). Cyclin D-Cdk4,6 Drives Cell-Cycle Progression via the Retinoblastoma Protein's C-Terminal Helix. *Molecular Cell*, *74*(4), 758-770.e4. https://doi.org/10.1016/j.molcel.2019.03.020
Vigo, T., La Rocca, C., Faicchia, D., Procaccini, C., Ruggieri, M., Salvetti, M., … Uccelli, A. (2019). IFNβ enhances mesenchymal stromal (Stem) cells immunomodulatory function through STAT1-3 activation and mTOR-associated promotion of glucose metabolism. *Cell Death and Disease*, *10*(2). https://doi.org/10.1038/s41419-019-1336-4
Wu, X., Dao Thi, V. L., Huang, Y., Billerbeck, E., Saha, D., Hoffmann, H. H., … Rice, C. M. (2018). Intrinsic Immunity Shapes Viral Resistance of Stem Cells. *Cell*, *172*(3), 423-438.e25. https://doi.org/10.1016/j.cell.2017.11.018
Wu, X., Kwong, A. C., & Rice, C. M. (2019). Antiviral resistance of stem cells. *Current Opinion in Immunology*, *56*, 50–59. https://doi.org/10.1016/j.coi.2018.10.004
Young, S. K., & Wek, R. C. (2016). Upstream open reading frames differentially regulate genespecific translation in the integrated stress response. *Journal of Biological Chemistry*, *291*(33), 16927–16935. https://doi.org/10.1074/jbc.R116.733899
Zhang, C., Cheng, N., Qiao, B., Zhang, F., Wu, J., Liu, C., … Du, J. (2020). Age-related decline of interferon-gamma responses in macrophage impairs satellite cell proliferation and regeneration. *Journal of Cachexia, Sarcopenia and Muscle*, *11*(5), 1291–1305. https://doi.org/10.1002/jcsm.12584
Zhu, X., Chen, Z., Shen, W., Huang, G., Sedivy, J. M., Wang, H., & Ju, Z. (2021). Inflammation, epigenetics, and metabolism converge to cell senescence and ageing: the regulation and intervention. *Signal Transduction and Targeted Therapy*, *6*(1), 1–29. https://doi.org/10.1038/s41392-021-00646-9
Zismanov, V., Chichkov, V., Colangelo, V., Jamet, S., Wang, S., Syme, A., … Crist, C. (2016). Phosphorylation of eIF2α is a Translational Control Mechanism Regulating Muscle Stem Cell Quiescence and Self-Renewal. *Cell Stem Cell*, *18*(1), 79–90. https://doi.org/10.1016/j.stem.2015.09.020